IN-19-CR
33461
P.54

Final Report

for the CSI GI Phase I Program
NASA Grants NAG 1-965 and NAG 1-1083

Experimental Demonstration of a Classical Approach for Flexible Space Structure Control: NASA CSI Testbeds

by

Bong Wie

Dept. of Mechanical & Aerospace Engineering
Arizona State University
Tempe, AZ 85287-6106

Prepared for

CSI Guest Investigator Program Office
NASA Langley Research Center
Hampton, VA 23665

August 31, 1991

Final Report

for the CSI GI Phase I Program
NASA Grants NAG 1-965 and NAG 1-1083

Experimental Demonstration of a Classical Approach for Flexible Space Structure Control: NASA CSI Testbeds

by

Bong Wie

Dept. of Mechanical & Aerospace Engineering
Arizona State University
Tempe, AZ 85287-6106

Prepared for

CSI Guest Investigator Program Office
NASA Langley Research Center
Hampton, VA 23665

August 31, 1991

Experimental Demonstration of a Classical Approach for Flexible Space Structure Control: NASA CSI Testbeds

Final Report
August 31, 1991

Grant Number: NAG 1-965 and NAG 1-1083

Period of Work: March 1, 1989 - August 31, 1991

Principal Investigator: Dr. Bong Wie
Dept. of Mechanical & Aerospace Engineering
Arizona State University
Tempe, AZ 85287-6106
(602) 965-8674

Submitted to: Ms. Rudeen Smith-Taylor
CSI Guest Investigator Program Office
NASA Langley Research Center
Hampton, VA 23665

Summary

This final report summarizes the results of active control experiments performed for the Mini-Mast truss structure at the NASA Langley Research Center and the ACES testbed at the NASA Marshall Space Flight Center, under the NASA CSI (Control Structure Interaction) Guest Investigator Program.

The primary research objectives were:

1. To develop active structural control concepts and/or techniques.

2. To verify the concept of robust non-minimum-phase compensation for a certain class of non-colocated structural control problems through ground experiments.

3. To verify a "dipole" concept for persistent disturbance rejection control of flexible structures.

4. To identify CSI issues and areas of emphasis for the next generation of large flexible spacecraft.

The classical SISO (single input and single output) control design approach was employed. The experimental results successfully demonstrate the simplicity and effectiveness of such a classical control design approach.

In particular, the effectiveness of a "dipole" concept for disturbance accommodating control of flexible structures has been successfully demonstrated for the ACES testbed which had been hampered by a nearly uncontrolled 0.15 Hz dominant mode. The HST (Hubble Space Telescope) pointing control problem caused by persistent solar-array excitation at 0.12 Hz and 0.66 Hz, which is very similar to the ACES's 0.15 Hz problem, is also discussed to support the significance of the experimental results accomplished for the NASA CSI testbeds.

Contents

* Proceedings of the 1990 American Control Conference, May 23-25, 1990, pp. 1428-1434, also *Journal of Guidance, Control, and Dynamics,* Vol.14, No. 4, March-April 1991, pp.778-784.

** Proceedings of the 1991 AIAA Guidance, Navigation, and Control Conference, August 12-14, 1991, pp. 818-826.

Classical Control System Design and Experiment for the Mini-Mast Truss Structure*

Bong Wie†
Arizona State University
Tempe, Arizona

Lucas Horta‡ and Jeff Sulla§
NASA Langley Research Center
Hampton, Virginia

Abstract

This paper describes control system design and experimental test results for the Mini-Mast truss structure located at the NASA Langley Research Center. Simple classical controllers and their ground test results are presented as a benchmark design for the Mini-Mast. The concepts of non-minimum-phase compensation and periodic disturbance rejection are experimentally validated. The practicality of a sensor decoupling approach for the classical single-input and single-output control design is also demonstrated. The test results which clearly indicate the undesirable effect of phase lag caused by computational delay and prefiltering are discussed.

*Proceedings of the 1990 American Control Conference, May 23-25, 1990, pp. 1428-1434, also Journal of Guidance, Control, and Dynamics Vol. 14, No. 4, March-April 1991, pp. 778-784.

†Associate Professor, Dept. of Mechanical and Aerospace Engineering, Associate Fellow AIAA.

‡Aerospace Engineer, Spacecraft Dynamics Branch, Member AIAA.

§Lockheed Engineering & Sciences Co., Hampton, VA.

Introduction

The objective of this paper is to describe control system design and the results of active control experiment performed for the Mini-Mast truss structure located at the NASA Langley Research Center, under the NASA CSI (Control Structure Interaction) Guest Investigator Program. The paper provides an overview of the Mini-Mast system, modeling for control design, control synthesis, and closed-loop test results. Simple classical controllers and their ground test results are presented as a benchmark design for the Mini-Mast. In particular, the simplicity and practicality of a classical control approach to the active structural control design are emphasized. Consequently, the theoretical aspects of large space structure control problems are not elaborated in this paper.

The Mini-Mast system [1] consists primarily of a 20-meter-long truss beam structure, which is deployed vertically inside a high-bay tower, cantilevered from its base on a rigid ground foundation. It represents future deployable trusses to be used in space. The overall system configuration and the actuator/sensor locations are illustrated in Fig. 1. Since this beam structure with significant tip mass is cantilevered to the ground, the overall transient responses are dominated by the first flexible mode in each axis. The 6-Hz second bending mode is widely separated from the 0.8-Hz first bending mode, and has an order-of-magnitude less modal contribution than the first mode. Following the second bending modes, there are a cluster of local modes and additional global bending, torsion, and axial modes up to 100 Hz.

Consequently, the Mini-Mast represents a typical control-structure interaction problem, where controlling the primary modes always requires consideration of the control interactions with the secondary modes. Even for a colocated actuator and sensor pair, special consideration must be given to the effect of the actuator and sensor dynamics and the phase lag caused by computational delay and prefiltering. In the preliminary control design, the first and second modes in each axis (except the second torsion mode) are considered as the primary modes to be actively damped. The third and higher modes in each axis are considered as the secondary modes which are not to be destabilized by the primary-mode controller.

The overall goals of Mini-Mast experiments described in this paper are: 1) a rapid transient control of the tip deflection to an impulsive disturbance, and 2) a steady-state vibration suppression to periodic disturbances. Control design and test results are presented for two different generic cases: 1) a colocated control using the tip-mounted

actuator and sensor pairs, and 2) a noncolocated control using the tip-mounted actuators and noncolocated sensors.

Mini-Mast System Description

In this section, the Mini-Mast system is briefly overviewed for the purposes of control design. As illustrated in Fig. 1, the basic element of the system is a 20-meter-long, triangular-cross-sectioned, joint-dominated truss structure. An approximately 160-kg tip mass includes three torque wheel actuators (TWA's) mounted on a tip plate at Bay 18; the total mass of the system is about 300 kg. A tensioned vertical cable serves to off-load the weight of the tip platform in order to prolong the fatigue life of the system; however, its effect on control experiments should be negligible.

The three TWA's generate orthogonal control torques along the global X, Y, and Z axes. The origin of the global control axes is located at the base of the truss and at the centroid of the triangular cross-section, as illustrated in Fig. 2. For disturbance input to the structure, three shakers at Bay 9 can be utilized. These shakers are oriented normal to the faces of the truss at each of the three vertices. Displacement sensors used for control experiments are located on the platforms at the tip (Bay 18) and near the mid-point of the truss (Bay 10). These sensors are positioned to measure deflections normal to the face of the sensor, which are mounted pararell to the flat face on the corner joints on the truss, as shown in Fig. 2. Since the sensor axes are not aligned with the torque wheel axes (i.e., the global X, Y, and Z axes), a coordinate transformation of the sensor outputs is needed for the classical decoupled control design. Such a coordinate transformation or sensor output decoupling matrix is given in Fig. 2.

Experimental, open-loop responses of the Mini-Mast excited by the shaker A with a pulse of 100 msec duration and 50 N magnitude are shown in Fig. 3 for the displacement sensor outputs (A, B, and C), and in Fig. 4 for the decoupled outputs (X, Y, and θ). It is evident from Fig. 3 that the overall transient responses at the tip are dominated by the first flexible mode in each axis. The 6-Hz second bending mode, which can be seen at Bay 10 responses, is widely separated from the 0.8-Hz first bending mode, and has an order-of-magnitude less modal contribution than the first mode. While there are a cluster of local modes and additional global bending, torsion, and axial modes up to 100 Hz, they are not visible in Fig. 3. The unsymmetric behavior of the Mini-Mast truss structure is also evident in this figure. This effect is probably due to the joint nonlinearity of the

truss structure. Despite such a joint nonlinearity problem, the decoupled outputs shown in Fig. 4 clearly indicate the effectiveness of the sensor decouplig concept illustrated in Fig. 2.

Although there are additional sensors, including accelerometers, distributed along the length of the truss, they are not utilized in the control experiments discussed in this paper.

A simplified transfer function representation of the actuator dynamics used for control design is given as [2]:

$$u(s) = \frac{s}{(s/s_1 + 1)(s/s_2 + 1)} u_c(s) \tag{1}$$

where $u(s)$ is the control torque in units of Nm; $u_c(s)$ is the torque wheel angular momemtum command in units of Nms; and s_1 and s_2 are the actuator poles. The following numerical values are used for control design: $s_1 = 25\ sec^{-1}$ and $s_2 = 300\ sec^{-1}$.

Mathematical Modeling for Control Design

A finite element model of the Mini-Mast truss structure developed in [1] consists of 355 joints and 490 beam elements. Rigid plates are positioned at Bays 18 and 10, with appropriate masses for the control hardware. Such a finite element model is represented by:

$$M\ddot{q} + Kq = f \tag{2}$$

where M is a positive definite mass matrix, K a positive semidefinite stiffness matrix, q a generalized nodal coordinate vector, and f a vector of external forces and/or torques. The above equation is transformed into the following modal equation:

$$\ddot{\eta} + \Omega^2 \eta = \Phi^T f \tag{3}$$

where η is a modal coordinate vector, $\Omega = \text{diag}(\omega_i)$, and ω_i is the ith modal frequency. Passive damping is often modeled with a modal damping matrtix.

A summary of the modal frequencies and modal damping ratios for the first five modes identified by modal tests is provided in Table 1. Modal damping ratios for the higher frequency modes are assumed to be 1 %. There are five modes below 10 Hz. The first two, at approximately 0.8 Hz, are first bending modes oriented nearly in the global X

and Y axes. Next is the first torsion mode at 4.4 Hz. It is slightly coupled with bending. The fourth and fifth modes are second bending modes. Unlike the first bending modes, however, the direction of motion for second bending has rotated 45 degrees from the global X- and Y-axes. This phenomenon results in the coupled second bending modes. Following the second bending modes, there are a cluster of 108 "local" modes. These modes involve mainly the bending of the diagonal truss members. Following this cluster of local modes, there are additional global bending, torsion, and axial modes up to 100 Hz. In the control design, the first five modes are considered as the primary modes to be actively damped. The sixth and higher modes are considered as the secondary modes which are not to be destabilized by the primary-mode controller.

Control Design Approaches and Objectives

State-space methods for control design of flexible space structures have been emphasized in the literature and more widely explored than classical methods. There has also been a growing research interest in robust H_∞ control and robustness analysis applied to the control problems of flexible space structures and the Space Station (e.g., see Refs. 3-5). However, the classical control approach [6-8] is employed for Mini-Mast control experiments and the objective is to investigate the fundamental nature of control-structure interaction problems and to further understand the practical effects of many simplifying assumptions on a realistic space truss structure such as the Mini-Mast.

In particular, a new concept of generalized structural filtering for flexible-mode stabilization, proposed in [8], and a periodic disturbance rejection concept, which are proposed for the Space Station Freedom [9] and further developed in [10-11], are to be validated by Mini-Mast control experiments. The simplicity and practicality of the classical control approach are to be demonstrated for the Mini-Mast. The practicality of a sensor decoupling approach is also to be demonstrated for the inherent multivariable control problem of the Mini-Mast.

The control objectives of Mini-Mast experiments described in this paper are: 1) a rapid transient vibration control of the tip deflection to an impulsive disturbance, and 2) a steady-state vibration suppression to periodic disturbances. Control design and tests are performed for two different generic cases: 1) a colocated control using the tip-mounted actuator and sensor pairs at Bay 18, and 2) a noncolocated control using the tip-mounted actuators at Bay 18 and noncolocated sensors at Bay 10. The external

disturbances are generated by shakers at Bay 9. In fact, there exists a multivariable control issue for both cases, since the sensor axes are not aligned with the control input axes. A sensor decoupling approach is, however, used to simplify the control design, which allows the use of a classical single-input single-output (SISO) control method.

In the next section, such a classical SISO control design approach is briefly reviewed, with a special emphasis on the concepts of generalized structural filtering and periodic disturbance rejection.

Classical Control Design

Generalized Structural Filtering Concept

In general, the classical gain/phase stabilization concepts are very useful for designing a SISO compensator. These classical control concepts are now significantly enhanced by the new concept of generalized structural filtering, especially with *non-minimum-phase zeros* [8]. A generalized second-order filter with arbitrary complex poles and zeros is simply represented as:

$$\frac{s^2/\omega_z^2 + 2\zeta_z s/\omega_z + 1}{s^2/\omega_p^2 + 2\zeta_p s/\omega_p + 1} \tag{4}$$

By different choices of the coefficients, several well-known frequency shaping filters can be realized. For $\omega_z = \omega_p$ and $\zeta_z = 0$, we have a notch filter for gain stabilization. The notch sharpness depends on the damping ratio of the notch pole. Great care must be exercised in selecting the parameters of the notch filter because of its phase lag at low frequency and its sensitivity to frequency uncertainty. For $\omega_p > \omega_z$ (and usually $\zeta_p = \zeta_z$), we have a complex phase-lead filter for phase stabilization. The amount of phase lead depends primarily on the ω_p/ω_z ratio, but the ratio should not be too high because of the gain increase at higher frequencies. Without the filter zeros, we have a simple roll-off filter.

Those filters discussed above are minimum phase, i.e., the filter poles and zeros are on the left-half s-plane. However, a variety of non-minimum-phase filters ($\zeta_z < 0$) studied in [8] have very interesting gain/phase characteristics which are useful for flexible-mode stabilization. The non-minimum-phase filtering, as opposed to the minimum phase filtering, provides the proper phasing to increase the closed-loop damping ratio of the flexible modes while maintaining a good robustness property to the model uncertainty [3, 4, 8].

Because of such a generalized structural filtering concept, the classical direct frequency shaping technique based on the gain/phase stabilization concepts is now significantly enhanced. Consequently, the design of a SISO compensator is simply carried out starting with the stabilization of the primary mode and subsequent analysis and stabilization of any unstably interacting flexible modes. Feedback control with a noncolocated actuator and sensor pair generally results in the presence of unstably interacting flexible modes. After the unstably interacting modes have been identified, proper filtering to phase or gain stabilize those modes is then introduced. Also, periodic disturbance rejection filtering is synthesized to compensate for any periodic disturbances acting on the structure. Aided by the root locus method and Bode plots, and a certain amount of trial and error, a robust compensator design is performed.

Active Disturbance Rejection

Active disturbance rejection control synthesis is simply achieved by introducing into the feedback loop a model of the disturbance [10-12]. It is assumed that a persistent disturbance with one or more frequency components is modeled as

$$w(t) = \sum_i A_i \sin(p_i t + \phi_i) \tag{5}$$

with unknown magnitudes A_i and phases ϕ_i but known frequencies p_i. The disturbance $w(t)$ can be described by a Laplace transformation $w(s) = N_w(s)/D_w(s)$, where $N_w(s)$ is arbitrary as long as $w(s)$ remains proper. The roots of $D_w(s)$ correspond to the frequency components of a periodic disturbance. The inclusion of the disturbance model $1/D_w(s)$ inside the control loop is often referred to as the internal modeling of the disturbance. In classical design, the internal disturbance model is regarded as being part of the compensator as shown in Fig. 5a.

The presence of $1/D_w(s)$ in the control loop results in the effective cancellation of the poles of w(s), provided that no root of $D_w(s)$ is a zero of the plant transfer function. This is shown in the following equations:

$$\begin{aligned} y(s) &= \frac{1/D(s)}{1 + N_c(s)N(s)/D_c(s)D_w(s)D(s)}\, w(s) \\ &= \frac{D_c(s)D_w(s)}{D_c(s)D_w(s)D(s) + N_c(s)N(s)}\, \frac{N_w(s)}{D_w(s)} \end{aligned} \tag{6}$$

As illustrated in Fig. 5b, the compensator can be viewed as a series of individual filters. Each filter is designed to perform a specific task, like the stabilization of a particular

mode for example. In the same manner, a disturbance rejection filter can be designed. That is, a numerator is properly chosen in the compensator to go together with the disturbance model as shown in Fig. 3b. The numerator is chosen to be of the same order as $D_w(s)$ so that there is a zero for each pole of the disturbance model. The presence of the disturbance model directly translates into a control input with components which will effectively cancel the periodic disturbance. Detailed discussions of both classical and state-space methods for periodic disturbance rejection control synthesis can be found in [9-11].

Although the active disturbance rejection concept based on the internal model principle has been well known (e.g, see Ref. 12), an interesting interpretation of the concept from a classical control viewpoint is given here. Each pole-zero combination of the periodic disturbance rejection filter can be called a "dipole." The filter thus consists of as many dipoles as there are frequency components in the periodic disturbance. The separation between the zero and the pole is generally referred to as the strength of the dipole. The strength of the dipole affects the settling time of the compensated system; the larger the separation between the pole and zero of the filter, the shorter the settling time is. This is caused by the position of the closed-loop pole corresponding to the disturbance frequency. As the strength of the dipole is increased, this pole is pushed farther to the left, speeding up the response time of the disturbance rejection. However, this separation influences the gain characteristics of the plant, since the dipole presents a certain amount of magnitude in the neighborhood of the pole and zero frequencies. Moreover, at frequencies higher than the dipole there is a net gain increase or reduction. The magnitude of this gain increases with the separation between pole and zero. Therefore, as the strength of the dipole is changed to meet a chosen settling time, the compensation must be readjusted. A compromise has to be reached often between the settling time and the stability of the closed-loop system [10-11].

Colocated Control Design and Experiments

A simplified control loop block diagram is shown in Fig. 6 for colocated control experiments using the tip-mounted actuators and displacement sensors A, B, and C at Bay 18. The sensor outputs are low-pass filtered by an analog, 3-pole Bessel filter with a corner frequency of 50 Hz in each axis. (Although a 50 Hz filter was used in the control design, it was found during the final stages of testing that a 20 Hz filter was mistakenly

selected. The resulting effect was significant and will be discussed later in this section.) The global X- and Y-axes bending and Z-axis torsional displacements at Bay 18 are generated by using the output decoupling matrix given in Fig. 2. The Y/u_1 transfer function has alternating poles and zeros along the imaginary axis. The X/u_2 and θ/u_3 transfer functions also have such a colocated actuator-sensor property. As a result, a SISO colocated control design is possible, where the TWA's at the tip provide the control inputs and the global displacements of the tip (Bay 18) are fed back with proportional gains. Thus, direct feedback of the decoupled displacement outputs (X, Y, θ) is the basic element of the colocated control experiments for the Mini-Mast using the torque wheel actuators whose dynamics are characterized by Eq. (1). However, a proportional-and-derivative (PD) control is needed to effectively compensate the actuator dynamics at near its high-pass break frequency. The PD compensator zero is chosen near the actuator pole at s = -25. A mismatching of the actuator pole by the PD compensation zero is not significant. An effective control loop delay of 15 msec from digital control implementation with a sampling rate of 66.6 Hz is assumed. Such a time delay causes approximately 33 degree phase lag at the second bending mode frequency of 38 rad/sec (6.1 Hz).

To validate the concept of active disturbance rejection for flexible space structures, a case with a sinusoidal disturbance with known frequency of 15 rad/sec and unknown magnitude of 5 N is considered. Such a sinusoidal disturbance is generated by shaker A at Bay 9, and disturbance rejection for the X- and Y-axes bending at the tip is considered. The compensator for this case, given in Fig. 6, includes a dipole for periodic disturbance rejection with the pole at $s = \pm j15$ and the zero at $s = \pm j10$, so that the zero lies between two consecutive poles of the loop transfer function. Figure 7 shows the locus of closed-loop poles vs. the overall loop gain for the X-axis control loop with the periodic disturbance rejection filter dipole.

The first test of this colocated controller was to investigate the closed-loop behavior to an impulsive disturbance. Figure 8 shows the closed-loop tip response of this controller for the same impulse disturbance as for Figs. 3 and 4. A 20% active damping ratio for the first mode in each axis has been achieved, as predicted by design. However, an undesirable phenomenon is evident in Fig. 8; that is, the second bending modes become less stable. This anomaly, which was not predicted by design, was found to be caused probably by the mistakenly selected analog prefilter of 20 Hz (instead of 50 Hz) corner

frequency. Additional test results with a 50 Hz filter indicate less destabilization of the second bending modes, but the second bending modes were still gain stabilized. The late discovery of this problem prevented a redesign of the colocated controller.

The test cycle proceeded with the sinusoidal disturbance. It was demonstrated that a periodic disturbance rejection can be achieved for the outputs X and Y at Bay 18 [13]. In this case, the control inputs, u_1 and u_2, present a steady state oscillation caused by the dipole, which counteracts the periodic disturbance applied on the system.

Noncolocated Control Design and Experiments

A case of further interest is the case where the controller uses displacement sensors which are not located at the tip but at the mid-section (Bay 10), resulting in a noncolocated control configuration. Figure 9 shows a control system block diagram for this noncolocated case, with non-minimum-phase compensation and with periodic disturbance rejection filtering for X and Y at Bay 10.

Similarly to the colocated case, the sensor outputs are low-pass filtered by an analog, 3-pole Bessel filter with a corner frequency of 50 Hz in each axis. Then, the global X- and Y-axes bending and Z-axis torsional displacements at Bay 10 are generated by using the output decoupling matrix. The Y/u_1 transfer function has non-alternating poles and zeros along the imaginary axis. The X/u_2 and θ/u_3 transfer functions also have such a noncolocated actuator-sensor property. A SISO control design, however, is still possible, where the TWA's at the tip provide the control inputs and the global displacements at Bay 10 are fed back with proper compensation.

The test results [13], for a case where the Mini-Mast is excited by the shaker A with a pulse of 100 msec duration and 50 N magnitude, show that the noncolocated control system, shown in Fig. 9, without the disturbance rejection filter dipole, has a 15% damping ratio for the first mode in each axis.

To validate the concept of periodic disturbance rejection for flexible space structures even for the noncolocated case, a case with a sinusoidal disturbance with known frequency of 15 rad/sec and disturbance rejection for the X- and Y-axes bending at Bay 10 is considered. The compensator for this case, given in Fig. 9, includes a dipole for periodic disturbance rejection with the pole at $s = \pm j15$. The zero corresponding to the dipole is placed at $s = \pm j20$, between the consecutive poles of the dipole and the second bending mode.

Figure 10 shows the locus of closed-loop poles versus overall loop gain for the X-axis control loop with both non-minimum-phase compensation and the periodic disturbance rejection filter dipole. Test results shown in Figure 11 demonstrate that a periodic disturbance rejection can be achieved for the outputs X and Y at Bay 10. The shaker A is turned on at t = 5 sec and turned off at t = 20 sec. The closed-loop system is stable and the control inputs, u_1 and u_2 (at Bay 18), present a steady state oscillation caused by the dipole, which counteracts the periodic disturbance applied on the system (at Bay 9).

Discussion

In the preliminary control design for the Mini-Mast, the first and second modes in each axis (except the second torsion mode) were considered as the primary modes to be actively damped. The third and higher modes in each axis were considered as the secondary modes which are not to be destabilized by the primary-mode controller. However, during the test cycle, it became clear that active control (i.e., phase stabilization) of the second bending modes was not practical in the presence of significant phase lag caused by the analog prefilter and computational time delay. Consequently, the second bending mode in each axis were gain stabilized, which undoubtedly caused some transient performance degradation at Bay 10, as can be seen in Fig. 8. An approach to actively control the second bending modes is to employ a complex phase lead filter [8]; however, test constraints and unmodeled high frequency dynamics prevented further refinement of the simple classical colocated controller shown in Fig. 6.

In summary, despite the second bending mode anomaly, the concept of non-minimum-phase compensation for the noncolocated control problem and the periodic disturbance rejection filter concept were successfully demonstrated for the Mini-Mast. The effectiveness of the sensor decoupling concept was also successfully validated.

Conclusions

The active structural control design and experimental test results for the Mini-Mast truss structure located at the NASA Langley Research Center have been presented. The simplicity and practicality of a classical control synthesis approach, enhanced by the concepts of non-minimum-phase filtering and active rejection of persistent disturbances,

were demonstrated. The test results have shown that the Mini-Mast can be an excellent generic test bed for validating the active vibration control technology for future large space structures. An important lesson learned from the Mini-Mast experiment is that even the single-input and single-output, colocated control design is a non-trivial task in practice.

References

[1] Pappa, R. et al., "Mini-Mast CSI Testbed User's Guide," NASA Langley Research Center, Hampton, VA, March 23, 1989.

[2] Taylor, L.W. and Rainy, D.W., "Torque Wheel Actuator Dynamics: Mini-Mast CSI Testbed," NASA Langley Research Center, Hampton, VA, July 1989.

[3] Byun, K.-W., Wie, B., and Sunkel, J., "Robust Control Synthesis for Uncertain Dynamical Systems," AIAA Paper No. 89-3516, to appear in the *Journal of Guidance, Control, and Dynamics.*

[4] Wedell, E., Chuang, C.-H., and Wie, B., "Stability Robustness Margin Computation for Structured Real-Parameter Variations," *Journal of Guidance, Control, and Dynamics*, Vol. 14, No. 3, 1991, pp. 607-614.

[5] Byun, K.-W, Wie, B., Geller, D., and Sunkel, J., "New Robust H_∞ Control Design for the Space Station with Structured Parameter Uncertainty," AIAA Paper No. 90-3319, to appear in the *Journal of Guidance, Control, and Dynamics.*

[6] Wie, B. and Bryson, A.E., Jr., "Pole-Zero Modeling of Flexible Space Structures," *Journal of Guidance, Control, and Dynamics*, Vol.11, No.6, 1988, pp.554-561.

[7] Wie, B., "Active Vibration Control Synthesis for the COFS-I," *Journal of Guidance, Control, and Dynamics*, Vol.11, No.3, 1988, pp.271-276.

[8] Wie, B. and Byun, K., "New Generalized Structural Filtering Concept for Active Vibration Control Synthesis," *Journal of Guidance, Control, and Dynamics*, Vol.12, No.2, 1989, pp.147-154.

[9] Wie, B., Byun, K.-W., Warren, V.W., Geller, D., Long, D., and Sunkel, "New Approach to Attitude/Momentum Control for the Space Station," *Journal of Guidance, Control, and Dynamics*, Vol.12, No.5, 1989, pp.714-722.

[10] Wie, B. and Gonzalez, M., "Active Control Synthesis for Flexible Space Structures Excited by Persistent Disturbances," AIAA Paper No. 90-3427, to appear in the *Journal of Guidance, Control, and Dynamics.*

[11] Wie, B., Liu, Q., and Byun, K.-W, "Robust H_∞ Control Design Method and Its Application to a Benchmark Problem," presented at the 1990 American Control Conference, to appear in *Journal of Guidance, Control, and Dynamics.*

[12] Chen, C.T., *Linear System Theory and Design*, CBS College Publishing, 1984, pp.488-506.

[13] *CSI Phase I Guest Investigator Year-End Review*, CSI Program Office, NASA Langley Research Center, January 23-24, 1990, pp.97-121.

Table 1: Mini-Mast modal properties

Mode	Frequency (Hz)	Damping Ratio (%)
1st X-Bending	0.801	1.964
1st Y-Bending	0.801	1.964
1st Torsion	4.364	1.660
2nd XY-Bending	6.104	1.194
2nd YX-Bending	6.156	1.194

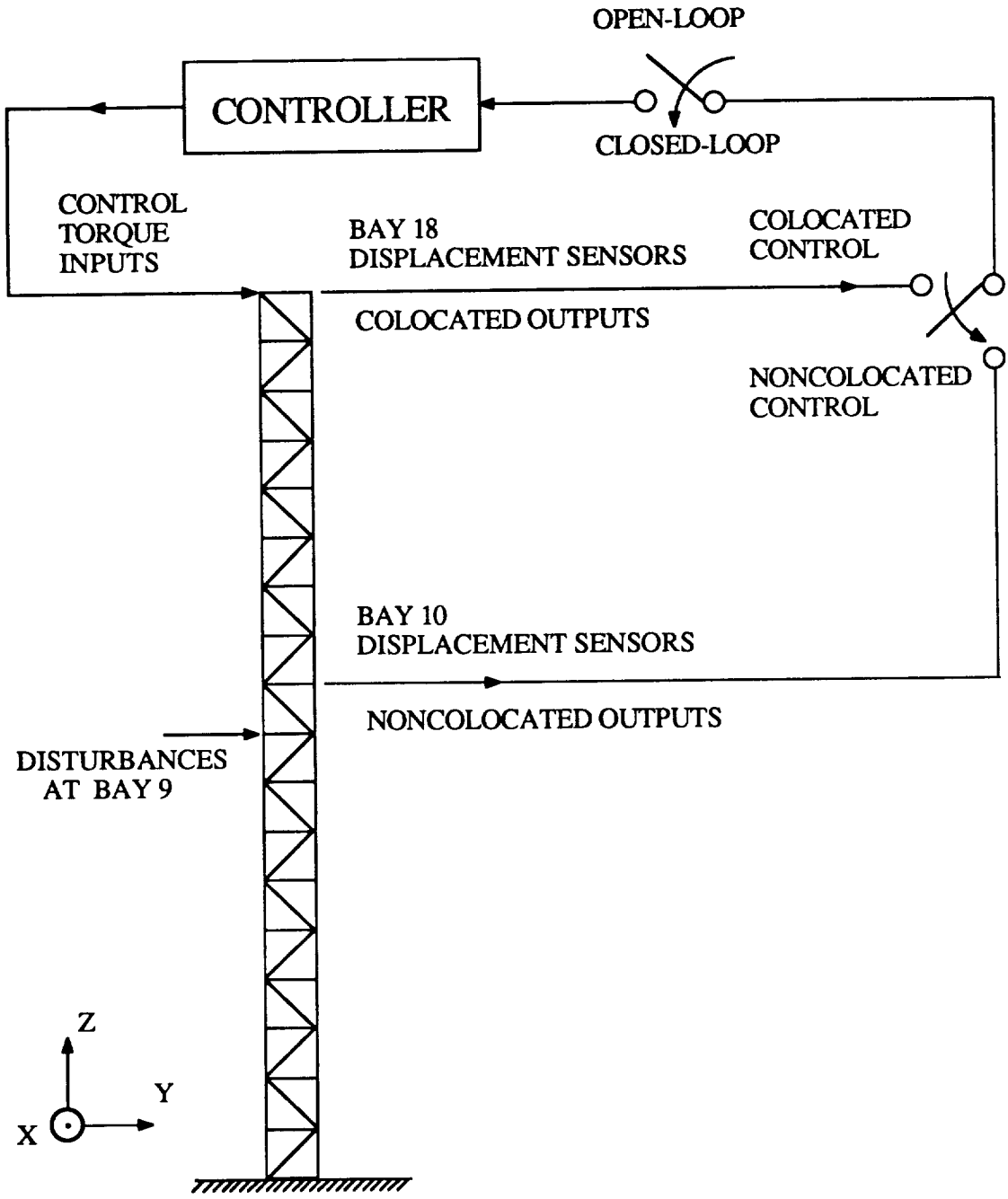

Figure 1. A schematic representation of Mini-Mast control experiments

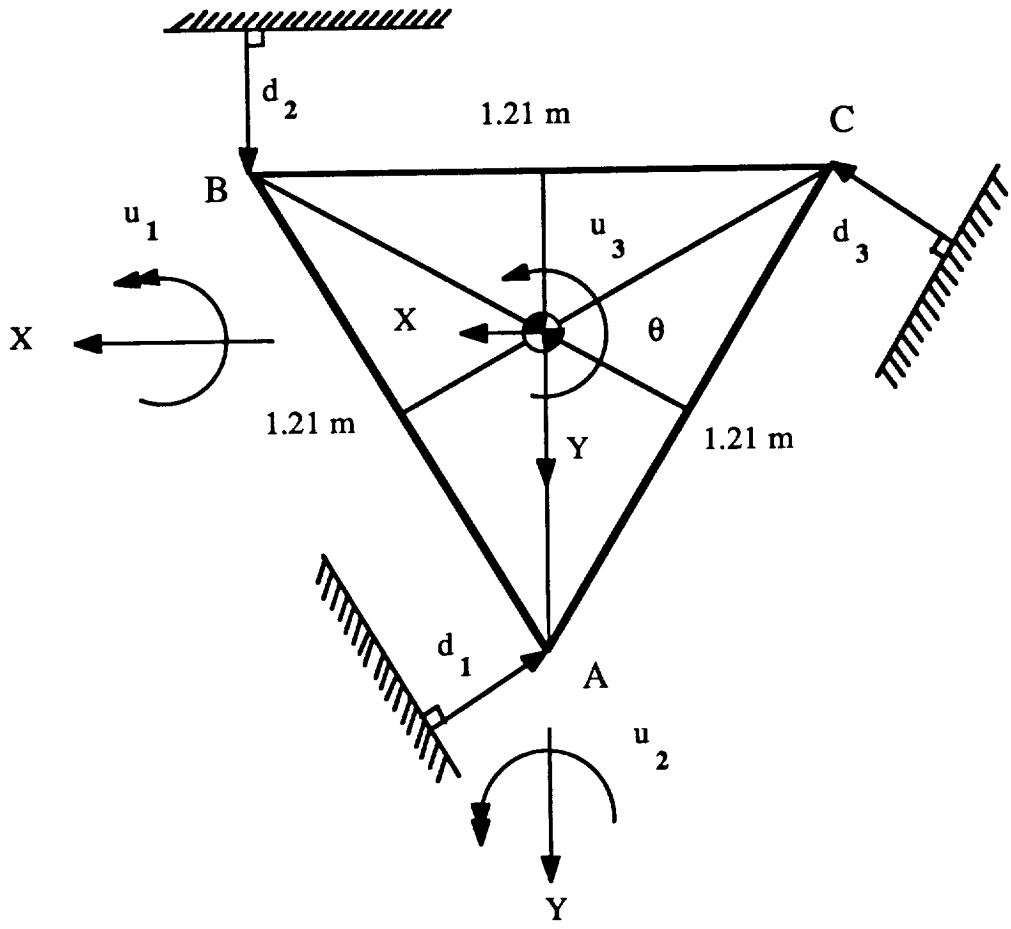

$$\begin{bmatrix} X \\ Y \\ \theta \end{bmatrix} = \begin{bmatrix} -0.57735 & 0 & 0.57735 \\ -0.3333 & 0.6666 & -0.3333 \\ 0.54986 & 0.54986 & 0.54986 \end{bmatrix} \begin{bmatrix} d_1 \\ d_2 \\ d_3 \end{bmatrix}$$

Figure 2. A schematic diagram of the Mini-Mast cross section and the decoupling matrix

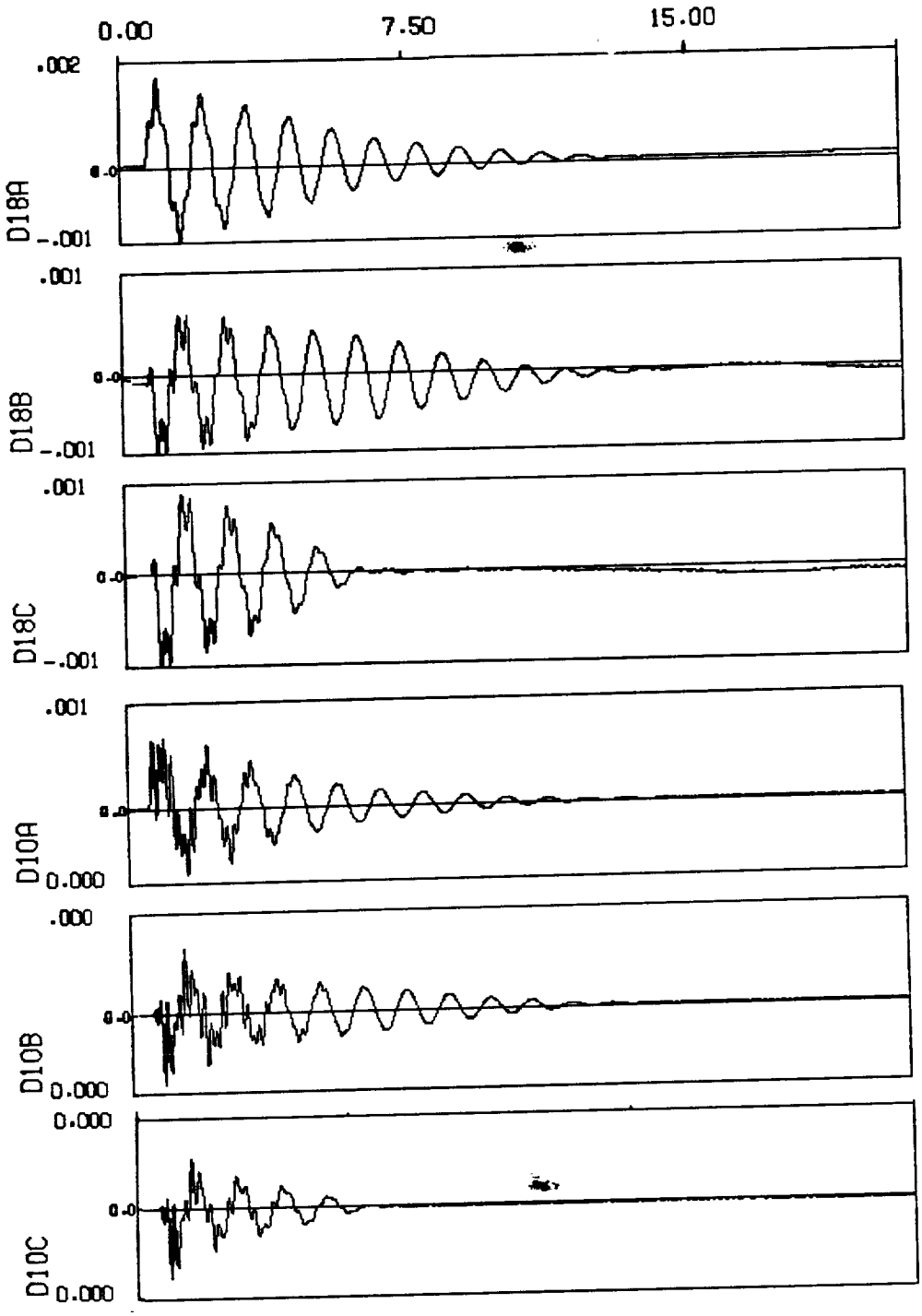

Figure 3. Open-loop impulse responses for displacement sensors A, B, and C at Bay 10 and Bay 18.

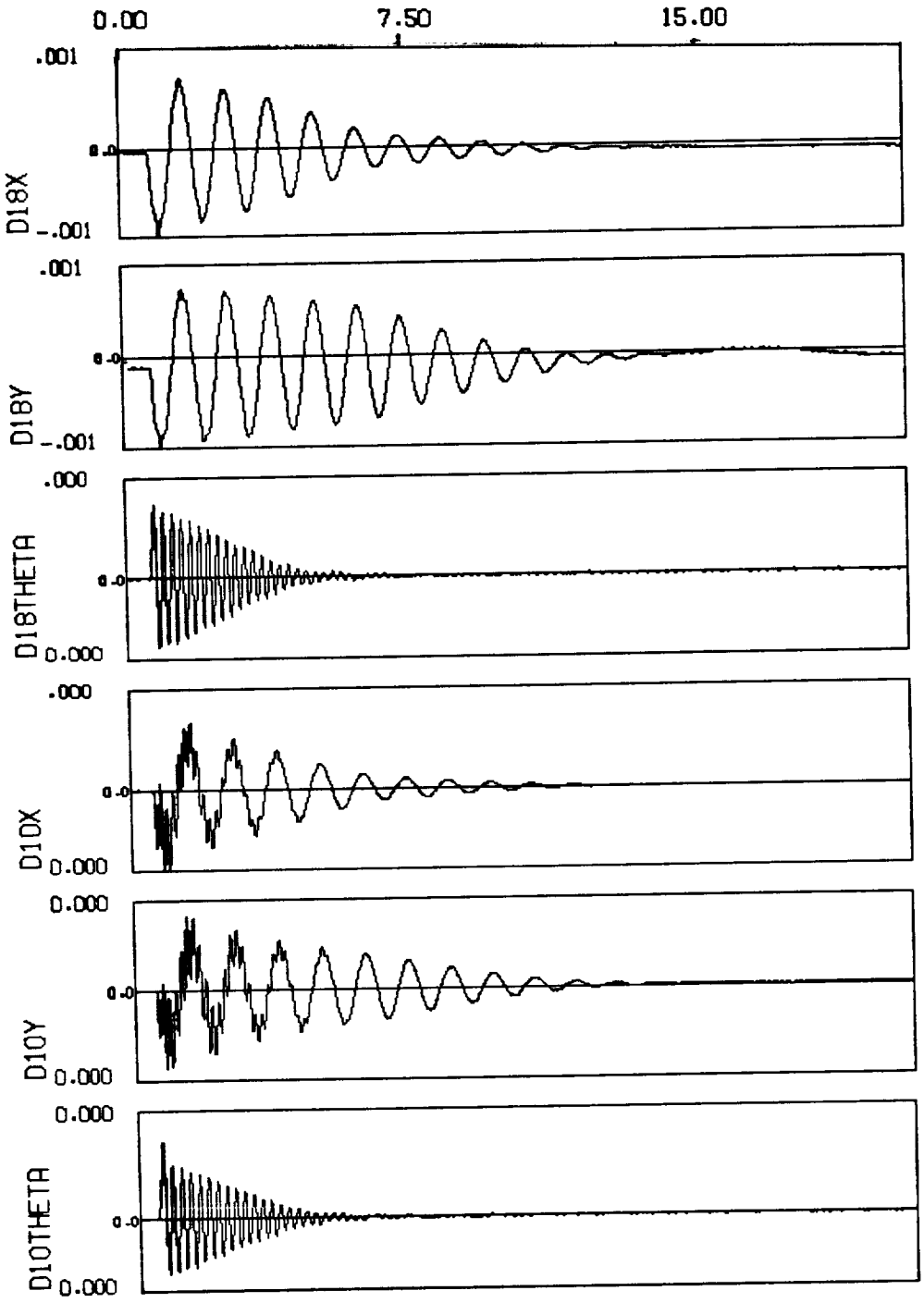

Figure 4. Open-loop impulse responses for decoupled outputs.

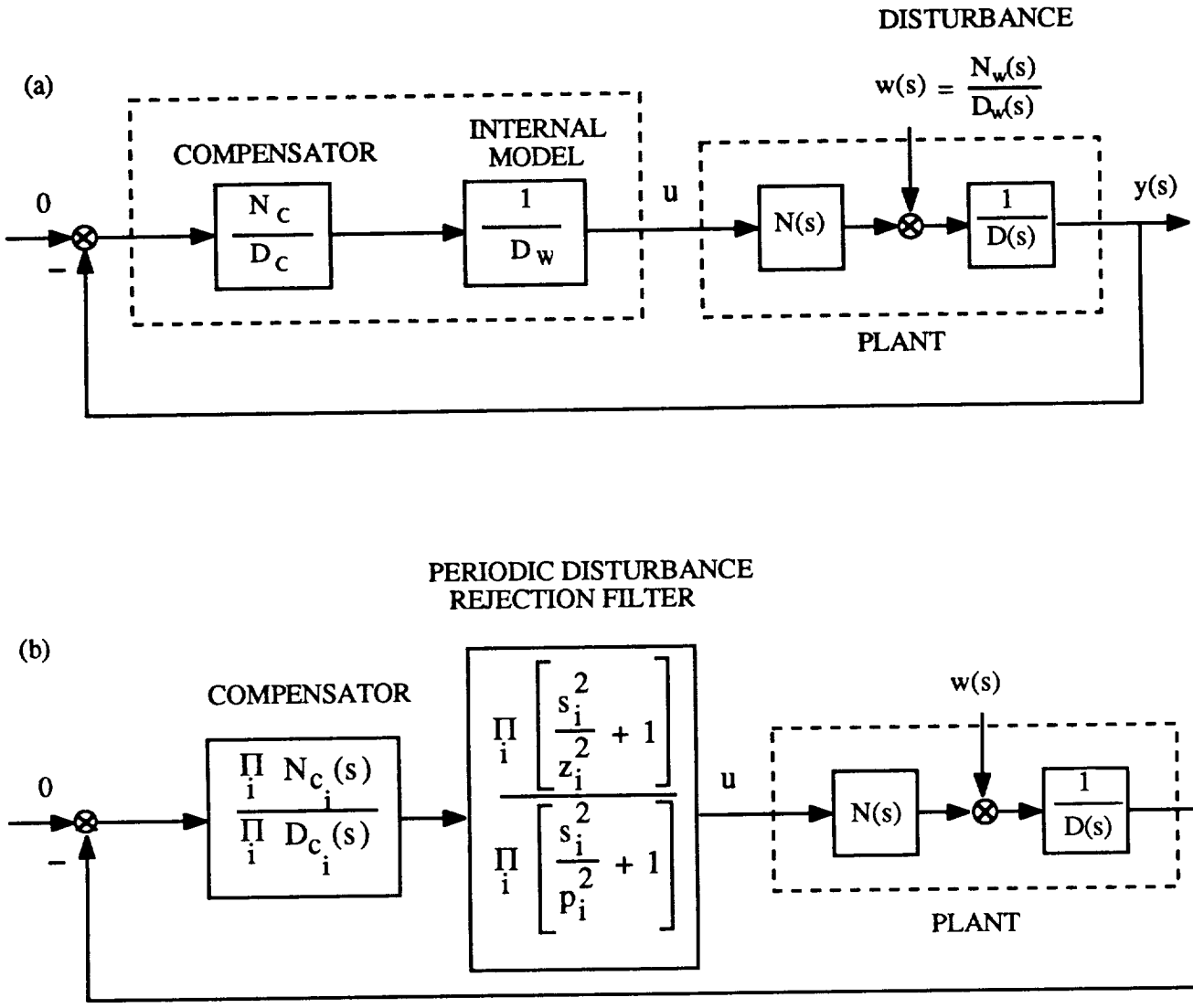

Figure 5. Block diagram representations of the periodic disturbance rejection controller

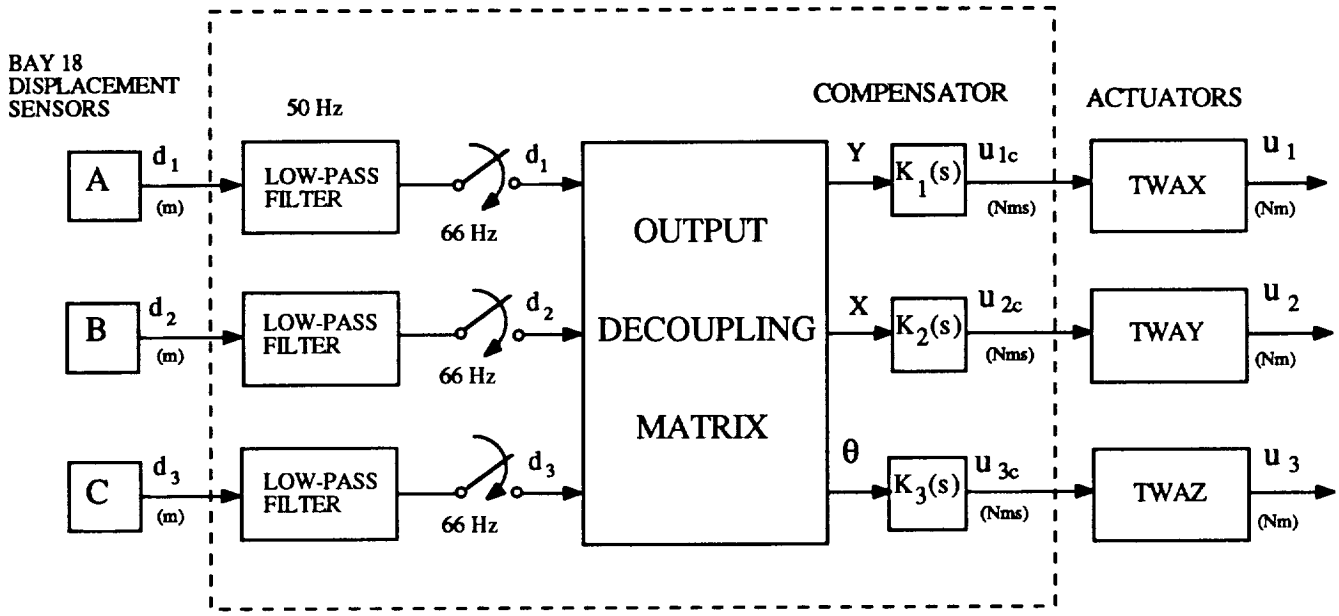

$$K_1(s) = -K_2(s) = \frac{4500\,(s/25+1)\,[(s/10)^2+1]}{(s/15)^2+1} \qquad K_3(s) = -800(s/25+1)$$

Figure 6. Colocated controller with periodic disturbance rejection filtering for X and Y at Bay 18

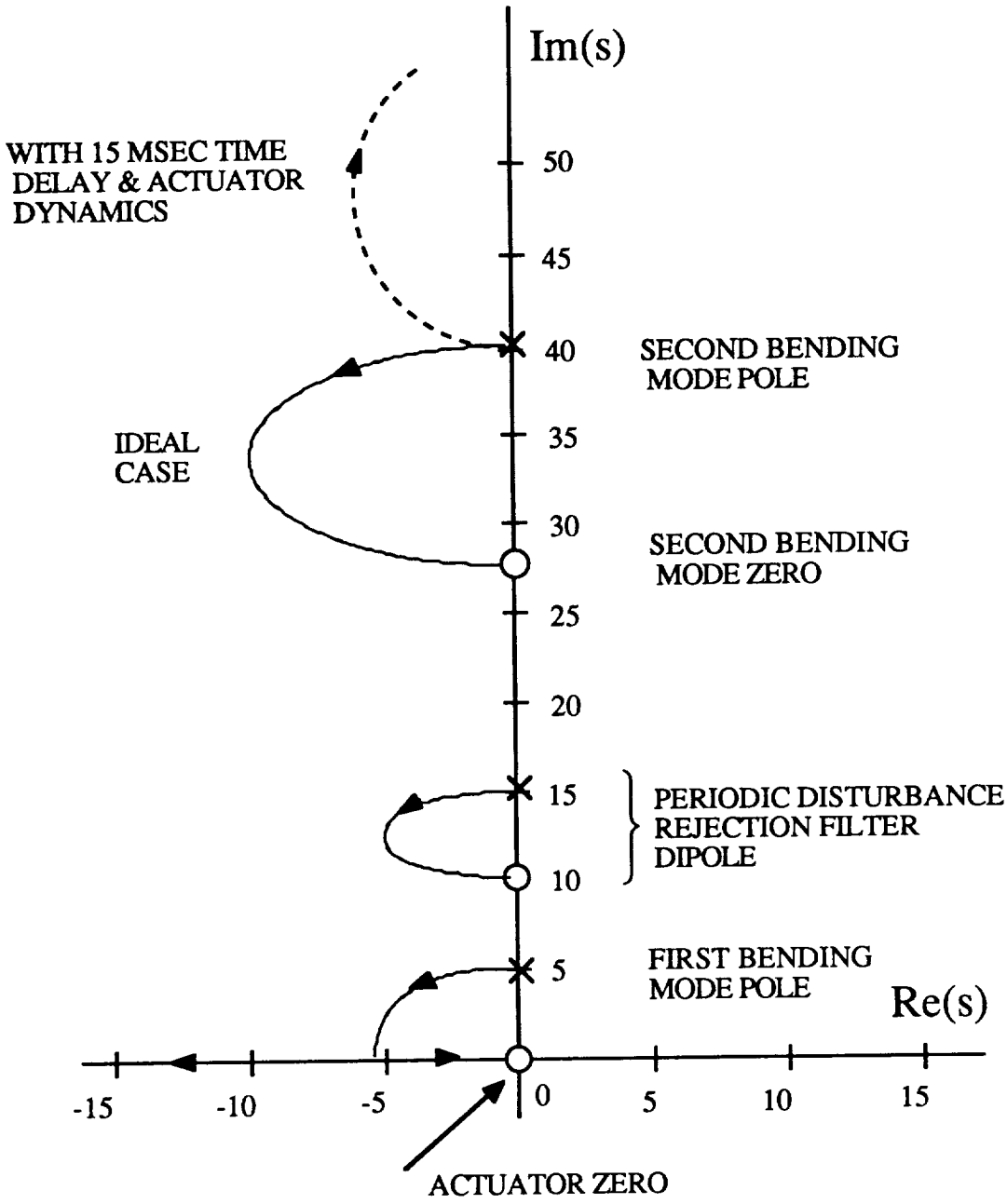

Figure 7. Root locus versus overall loop gain of the colocated X-axis controller

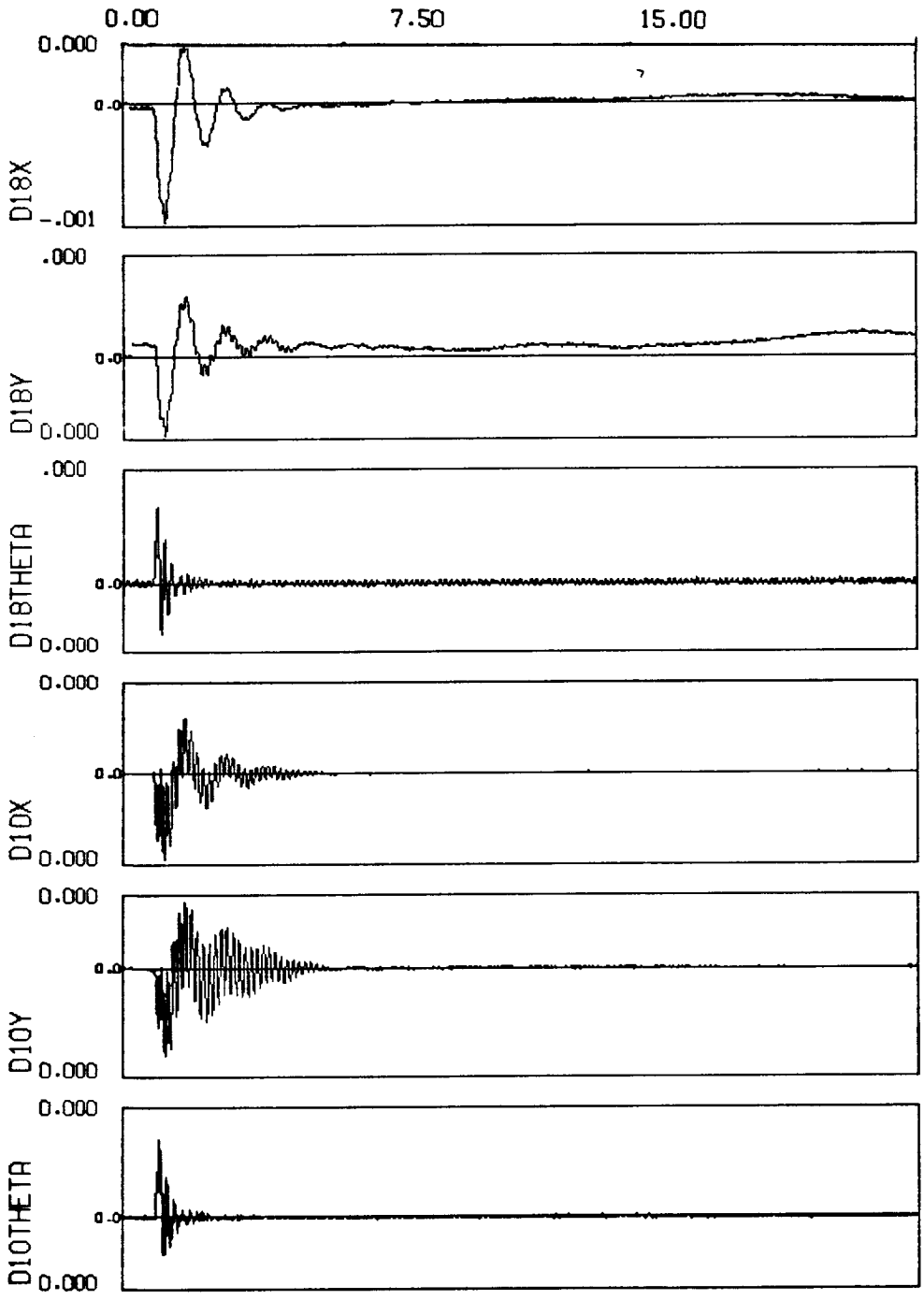

Figure 8. Closed-loop impulse responses of the collocated controller.

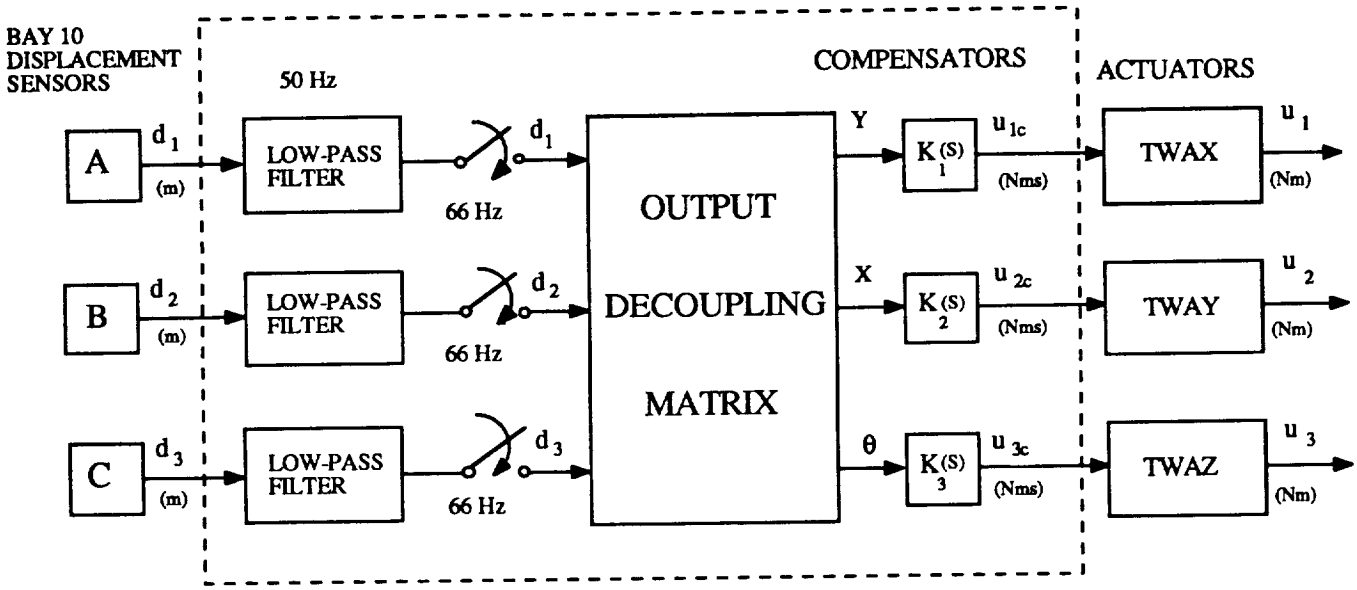

$$K_1(s) = -K_2(s) = \frac{-6000(s/25+1)[(s/20)^2+1][(s/4.9)^2-1.4s/4.9+1]}{[(s/15)^2+1][(s/4.9)^2+1.4s/4.9+1]}$$

$$K_3(s) = -800(s/25+1)$$

Figure 9. Noncolocated controller with periodic disturbance rejection filtering for X and Y at Bay 10

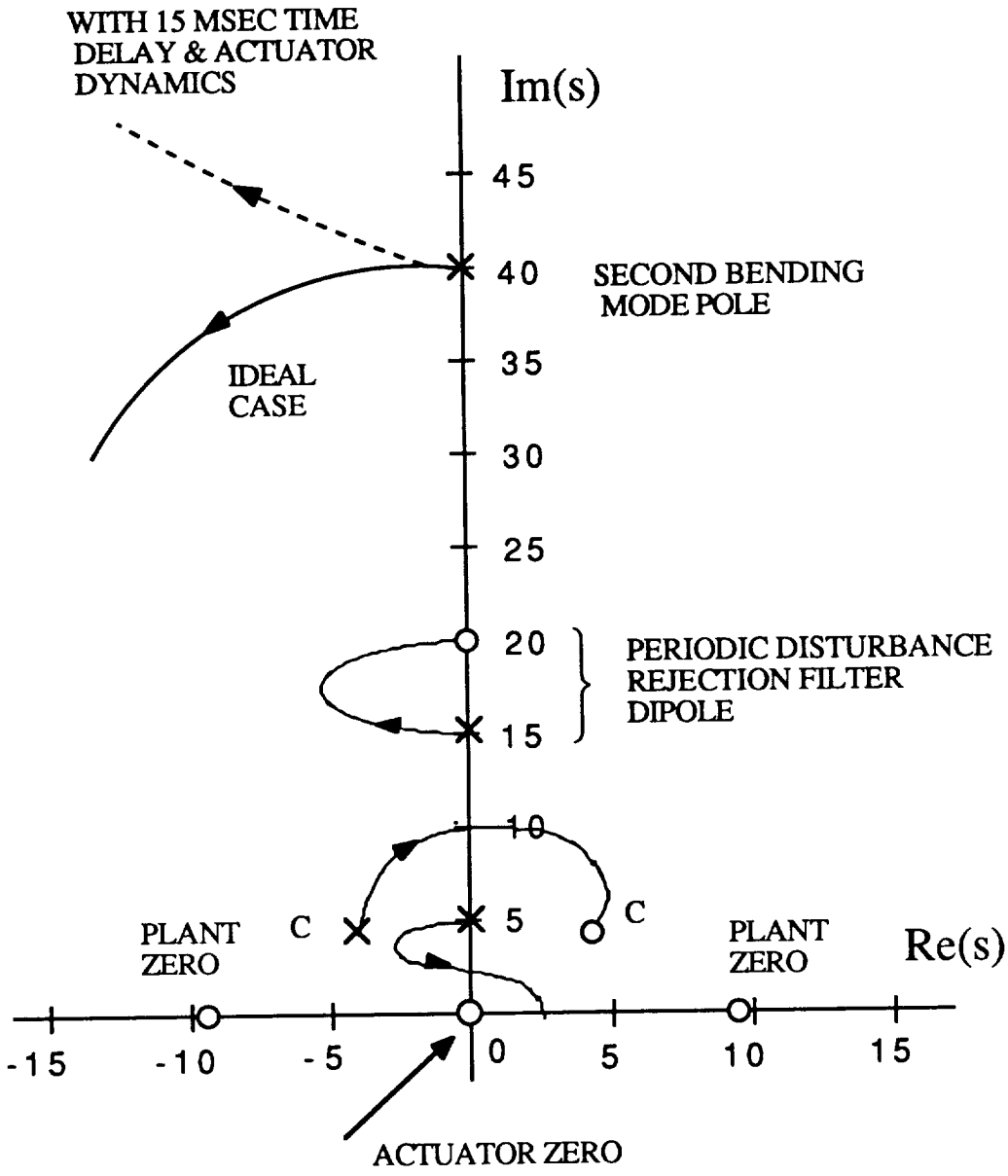

Figure 10. Root locus versus overall loop gain of the noncolocated X-axis controller

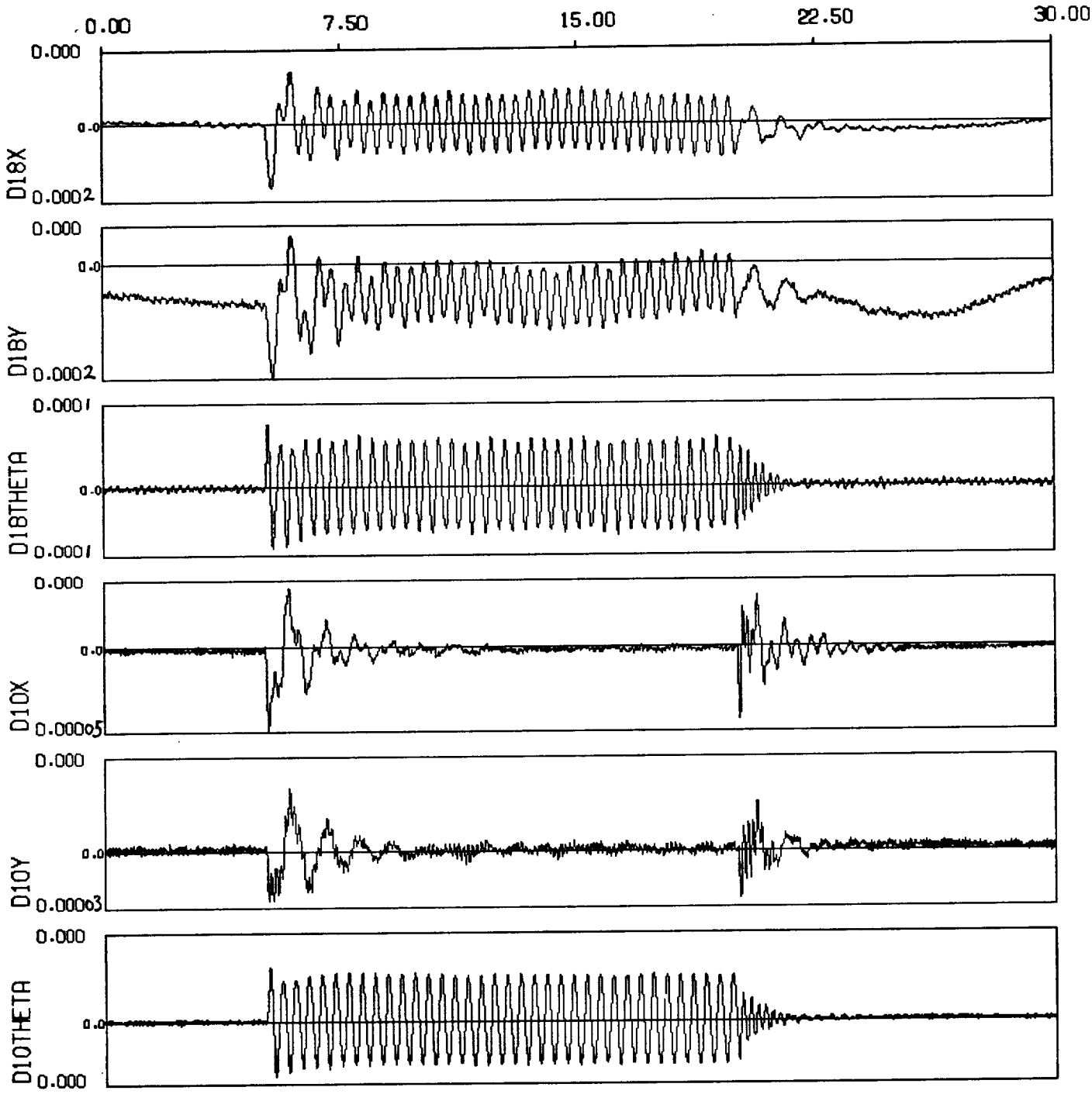

Figure 11. Closed-loop sinusoidal responses of the noncolocated controller with disturbance rejection for X and Y at Bay 10.

Experimental Demonstration of a Classical Approach for Flexible Structure Control: the ACES Testbed*

Bong Wie †
Arizona State University
Tempe, Arizona 85287-6106

Abstract

This paper describes the results of an active structural control experiment performed for the ACES testbed at NASA Marshall Space Flight Center as part of the NASA Control-Structure Interaction Guest Investigator Program. The experimental results successfully demonstrate the effectiveness of a "dipole" concept for line-of-sight control of a pointing system mounted on a flexible structure. The simplicity and effectiveness of a classical "single-loop-at-a-time" approach for the active structural control design for a complex structure such as the ACES testbed are demonstrated. Consequently, the theoretical aspects of large space structure control problems are not elaborated in this paper.

*Proceedings of the 1991 AIAA Guidance, Navigation, and Control Conference, August 12-14, 1991, pp. 818-826.

†Associate Professor, Dept. of Mechanical & Aerospace Engineering, Associate Fellow AIAA.

1. Introduction

This paper describes a ground experiment conducted for the Advanced Control Evaluation for Structures (ACES) testbed at the NASA Marshall Space Flight Center, under the NASA Control-Structure Interaction (CSI) Guest Investigator Program [1]. State-space methods for control design of flexible space structures have been emphasized in the literature and more widely explored than a classical method, as evidenced by *all* the prior control experiments conducted for the ACES [2-9]. However, this paper describes the results of testing a classical controller [10] for the ACES testbed. During tests, particular emphasis was placed on: 1) understanding the fundamental nature of control-structure interaction problems, and 2) exploring the effects of many simplifying assumptions on a realistic complex structure such as the ACES. Consequently, the theoretical aspects of large space structure control problems are not elaborated in this paper.

The overall objective of the CSI Program is to develop and validate the technology needed to design, verify, and operate advanced space vehicles with significant structural flexibility [1]. Some unique features of the technical approach employed to meet such overall objectives and to accomplish a successful experiment are summarized as follows:

1) A classical "single-loop-at-a-time" control design approach [11-14] was employed for the ACES with multiple actuators and sensors, while modern state-space multivariable control design approaches were employed in [2-9].

2) *Analytical* models were used for the classical control design, while experimentally identified, state-space models were used for the state-space control designs in [6-9].

4) The primary goal of verifying the simplicity of the classical control design approach for flexible structure control in achieving moderate performance and stability, with minimum controller complexity and minimum design efforts, has been accomplished, as evidenced by the experimental results compared with the test results presented in [2-9].

5) In particular, the simplicity and effectiveness of a "dipole" concept for disturbance accommodating control of flexible structures [13,14] has been successfully demonstrated for the ACES testbed which had been hampered by an "uncontrolled" 0.2 Hz dominant mode [2-5].

The remainder of this paper is organized as follows. Section 2 describes the ACES test facility. Section 3 discusses classical control design for the ACES and Section 4

presents the experimental results. Section 5 further discusses some fundamental issues in control design for large space structures. In Section 6, the "dipole" concept, successfully demonstrated for the ACES, is proposed for the Hubble Space Telescope with a pointing control problem caused by persistent solar-array excitation at 0.12 Hz and 0.66 Hz [15], which is very similar to the ACES's 0.2 Hz problem. In the Appendix, the classical control design approach employed for the experiment is summarized.

2. The ACES Testbed

In this section, the ACES testbed and its objectives are briefly described. A detailed description of the ACES facility and previous experimental results by other control researchers can be found in [2-9].

ACES System Description

The basic configuration of the ACES test facility is shown in Fig. 1. The basic component is a 2.27-Kg, 13-meter deployable Astromast which served as the flight backup magnetometer boom for the Voyager spacecraft. It is a symmetric beam which is triangular in cross section. The Astromast has the equivalent continuous beam parameter of EI $= 2.31e8\ Nm^2$. Appendages are attached to the Astromast to emulate the closely-spaced modal frequencies characteristic of large space structures. The appendages consist of an antenna and two counterbalance legs. The overall system has 43 structural modes under 8 Hz. Table 1 lists some of the dominant modes of the ACES structure.

The Base Excitation Table (BET) is hydraulically driven to provide two-axis translational disturbances at the point where the Astromast is attached to the overhead structure of the building. Several disturbances, representative of an actual space environment, can be provided by the BET. Later in this paper, two of these disturbances utilized in the experiment will be referred to as: 1) BET pulse (thruster firings) and 2) BET step (crew motion disturbance).

The Advanced Gimbal System (AGS) is a precision, two-axis gimbal system designed for high accuracy pointing applications, augmented by a third gimbal with a torquer and air-bearing system for azimuth control. The AGS provides torque actuation at the base mounting plate of the Astromast in response to voltage command over the range of ± 10 Volts. The AGS torquers operate over ± 30 degrees, saturate at 50 Nm of torque, and have bandwidths in excess of 50 Hz. Rate gyros are provided at the base and tip of the

Astromast, and they measure three-axis angular rates at each location. The AGS and the rate gyros at the base become co-located actuator/sensor pairs.

The Linear Momentum Exchange Devices (LMED) are proof-mass actuators which produce translational forces in two-axes at each location, as shown in Fig. 1. Each LMED has a co-located accelerometer and a proof-mass position transducer. The moving mass of 0.75 Kg contains permanent magnets which can move ± 3 cm over a voice coil actuator driven by a constant current source amplifier. Each LMED can deliver a peak force of 90 N; however, over the ± 10 Volt range of the control input, a maximum continuous force of 18 N is available. The force applied to the proof mass appears as a reaction force to the structure.

An optical system is provided to measure two-axis angular displacement of the antenna frame and thus monitor the line-of-sight pointing performance. The system consists of a laser source, two mirrors, and a two-axis optical detector. One of the mirrors is mounted on a two-axis pointing gimbal so the system can be used as a closed-loop Image Motion Compensation (IMC) controller in addition to an optical performance sensor. The objective of this setup is to test an IMC controller which will minimize the laser-beam pointing error; this setup is representative of a secondary-mirror pointing control system of a large telescope.

A digital computer with a sampling rate of 50 Hz is provided to implement digital controllers and to store and post-process test results.

The ACES Tetbed Objectives

Similar to control experiments reported in [2-9], the primary goals of control design to be verified for the ACES testbed were:

1) to reduce the IMC line-of-sight error (i.e., to point the laser beam in the center of the detector) in the presence of two representative disturbances,

2) to ensure that the controller has a practical size,

3) to ensure that the controller is tolerant of model uncertainties.

The performance measures employed to evaluate the controller effectiveness include the detector response, the base rate gyro response, and the controller complexity. The primary performance criterion was the IMC line-of-sight pointing accuracy.

During the previous experiments conducted by other researchers for the ACES [2-5], several problems were encountered. One of such problems was described in [4] as:

"An unmodeled mode appeared as the dominant mode at the detector. Since the detector error was intended to be the evaluation parameter, the appearance of the unmodeled mode was disastrous to the original evaluation plan. The mode (0.2 Hz) did not destabilize any of the controllers; on the other hand, no controller attenuated the mode."

This 0.2 Hz mode problem, however, was not encountered by other CSI Guest Investigators (e.g., see [6-9]) since their controllers were not tested for the so-called BET step disturbance which is one of three representative disturbances available for the ACES.

One of the major contributions of this paper is to show that such a control problem encountered during the previous experiments was actually caused by the "nearly uncontrollable" but "significantly disturbable" 0.2 Hz mode (to be precise, it is a 0.15 Hz mode). The mode is nearly uncontrollable by the AGS torque input and completely uncontrollable by the IMC gimbals. However, it can be excited or disturbed significantly by the BET step disturbance and can be observed by the IMC detector.

This paper will show that a simple IMC controller utilizing the "dipole" concept [13,14] can easily rectify such an "uncontrolled" mode problem. This paper will also show that the pointing control problem recently encountered by the Hubble Space Telescope [15] is very similar to the ACES control problem with the "uncontrolled" dominant mode. Consequently, a simple controller utilizing the dipole concept is proposed for the Hubble Space Telescope.

3. Classical Control Design

The first step in control system design is to obtain a mathematical model of the physical system to be controlled. In general, a finite element model of a flexible structure is represented by

$$M\ddot{q} + Kq = f \tag{1}$$

where M is a positive definite mass matrix, K a positive semidefinite stiffness matrix, q a generalized nodal coordinate vector, and f a vector of external forces and/or torques.

Equation (1) is transformed into the modal equation:

$$\ddot{\eta} + \Omega^2\eta = \Phi^T f \tag{2}$$

where η is a modal coordinate vector, $\Omega = \text{diag}(\omega_i)$, and ω_i the ith modal frequency, and Φ the modal matrix.

The math model of the ACES provided by the NASA Marshall Space Flight Center includes the modal frequencies and mode shapes of the lowest 43 modes, and transfer function models of the ACES were used for classical control design.

Figure 2 illustrates a classical control system architecture selected for the ACES. Basically, the control system consists of 6 actuators and 6 sensors without cross feedback. The control inputs are the X- and Y-axis torques of the AGS gimbals, the X- and Y-axis forces of LMED located at the lower section of the Astromast, and X- and Y-axis torques of the IMC gimbals. The sensor measurements consist of the X- and Y-axis base rate gyros (BGYRO), the X- and Y-axis accelerometer (ACC) outputs of the LMED, and the X- and Y-axis detector (DET) position outputs.

The classical "single-loop-at-a-time" control design for the ACES is briefly described as follows:

1) The AGS-X to BGYRO-X (also the AGS-Y to BGYRO-Y) loop basically consists of a co-located torque actuator and angular rate sensor pair. Although the effect of phase lag at high frequencies, caused by actuator/sensor dynamics and control loop time delay, must be considered in practical control design, a co-located direct rate feedback controller, as shown in Fig. 2, was chosen for testing. Because of relatively weak cross-axis coupling, it is not necessary to cross feedback the BGYRO outputs to the AGS gimbals.

2) The IMC-X to DET-Y (also the IMC-Y to DET-X) transfer function plot [2] includes a few flexible modes near 1.5 Hz. As a result, a classical PID controller, as shown in Fig. 2, was chosen for each IMC loop. Similar to the AGS loops, it is not necessary to cross feedback the detector (DET) outputs to the IMC gimbals.

3) As can be seen in Fig. 2, a direct acceleration feedback with first-order roll-off filtering was chosen for each co-located LMED and acceleration (ACC) control loop [11].

It is important to note that the baseline controller shown in Fig. 2 was designed without consideration of the unmodeled 0.15 Hz mode, which will be discussed later. In the Appendix, a classical single-input single-output (SISO) control design approach is summarized, with special emphasis on the concept of periodic disturbance rejection using a "dipole," which will be shown to be very effective for accommodating the 0.15 Hz mode disturbance.

4. Experimental Results

In this section, some of the experimental results are presented, which support the effectiveness of a simple classical controller, shown in Fig. 2, for achieving an excellent closed-loop performance.

Figure 3 shows a direct comparison of the open-loop and AGS closed-loop responses of BGYRO-X to a BET-Y pulse disturbance. Figure 3a shows the BGYRO-X open-loop response dominated by a 2.3 Hz mode. It can be seen in Fig. 3b that the 2.3 Hz mode is actively damped by the AGS controller (with nominal gain). However, an undesirable phenomenon of high-frequency instability is evident in Fig. 3c when the AGS rate gain is increased by a factor of two for more active damping of the 2.3 Hz mode. This experimental result confirms that there is no such a case as a perfect "co-located" rate feedback control with an infinity gain margin. Consequently, the AGS controller with nominal gain has a 6 dB gain margin.

Figure 4 shows a direct comparison of the open-loop and AGS closed-loop responses of DET-X to a BET-X pulse disturbance. Figure 4a shows the open-loop response of the detector output, dominated by two structural modes at 0.75 Hz and 2.3 Hz. As can be seen in Fig. 4b, significant performance improvement is achieved by the AGS controller (with nominal gain). Both the 0.75 Hz and 2.3 Hz modes are effectively damped out by the "co-located" rate feedback controller in the detector response.

Figure 5 shows the closed-loop responses of DET-X to a BET-X pulse disturbance. Figure 5a demonstrates the effectiveness of controlling the 2.3 Hz mode (but not the 0.75 Hz mode) by the LMED. As can be seen in Fig. 5b, very significant performance improvement in both the line-of-sight error and vibration suppression is achieved by the integrated AGS and IMC controller, as compared to the open-loop response shown in Fig. 4a.

Based upon the experimental results summarized as in Figs. 3-5, it may be fair to say that an excellent closed-loop performance has been achieved by a rather *simple* classical controller shown in Fig. 2, compared to other experimental results reported in [2-9].

However, a case of further interest is the case with the BET step disturbance. Figure 6 compares the open-loop and closed-loop responses of DET-X to a BET-X step disturbance. Figure 6a shows the open-loop response, dominated by a 0.15 Hz mode and other lower frequency modes. Figure 6b shows the baseline integrated IMC/AGS closed-loop

response, which is undoubtedly unacceptable. The reason for such unacceptable (also unpredicted) closed-loop performance is due to the presence of the 0.15 Hz mode (called 0.2 Hz mode in [2-5]) which can be seen in both Fig. 6a and Fig. 6b.

Several prior ACES experiments had been hampered by the "uncontrolled" 0.15 Hz mode [2-5]. It is important to note that such a low frequency mode is nearly uncontrollable by the AGS torque input, nearly unobservable by the base rate gyros, and completely uncontrollable by the IMC gimbals. However, it can be excited or disturbed significantly by a BET step disturbance and can be observed by the IMC detector which is not co-located with the AGS and the rate gyros at the base.

For the purpose of IMC controller redesign, the 0.15 Hz mode excitation can be simply considered as a persistent external disturbance. To isolate such an undesirable disturbance, a new IMC controller shown in Fig. 7 was designed. The new controller simply includes a dipole for disturbance rejection with the pole at $s = \pm j0.9$. The zero corresponding to the dipole is placed at $s = \pm j0.1$. A detailed discussion of this dipole concept can be found in the Appendix.

The closed-loop test result shown in Fig. 6c clearly demonstrates the effectiveness of the redesigned IMC controller for rejecting the 0.15 Hz mode in the detector output.

5. Discussion

State-space methods for control design of flexible space structures have been emphasized by many control researchers and more widely explored than classical methods (e.g., see [2-9]). This arises from the convenience of obtaining a compensator for the whole system given one set of weighting parameters. However, the fundamental question remains how to choose these parameters and what choice provides the "best" optimal design. The designer must find an acceptable set of parameters for a "good" optimal design. The use of state-space methods for control design usually results in a compensator of the same order as the system to be controlled. This means that for systems having several flexible modes, the compensator adds compensation even to modes that are stable and need no compensation. This may result in a high-order compensator design.

In classical design, on the other hand, a compensator must be constructed piece by piece, or mode by mode. As demonstrated in the preceding sections, the classical design is particularly convenient for the control of flexible space structures with properly

selected "co-located" actuator/sensor pairs. The concept of non-minimum-phase compensation also provides an extremely convenient way of stabilizing unstably interacting flexible modes for the case in which actuators and sensors are not co-located, as discovered in [12] and also as demonstrated experimentally in [14]. The resulting compensator is usually of less order than the system to be controlled since not all flexible modes in a structure tend to be destabilized by a reduced-order controller.

A helpful characteristic of most flexible space structures is their inherent passive damping. This gives the designer the opportunity of phase stabilizing significant modes and to gain stabilize all other higher frequency modes which have less influence on the structure, as demonstrated in the preceding sections (e.g., see Fig. 3).

6. The HST Pointing Control Problem

In this section, the solar-array thermal flutter problem of the Hubble Space Telescope (HST) is briefly discussed to emphasize the significance of the experimental results for the ACES in accommodating the 0.15 Hz disturbance. Detailed discussions of the HST pointing control system and its solar-array excitation problem can be found in [15-18]

According to Ref. [15], there appear to be two types of thermal flutter of the 20-ft-long solar arrays: 1) an end-to-end bending oscillation at 0.12 Hz when the spacecraft passes between sunlight and shadow, and 2) a sideways bending oscillation at 0.66 Hz that occurs on the day side of the Earth. The effect of such solar-array vibration is that the pointing performance of the spacecraft is significantly degraded, especially, in the pitch and yaw axes.

The HST can be represented in transfer-function form for each control axis as follows:

$$\frac{\theta(s)}{u(s)} = \frac{1}{Is^2} + \sum_{i=1} \frac{K_i/I}{s^2 + 2\zeta\omega_i s + \omega_i{}^2} \tag{3}$$

where θ is the attitude error output, u the reaction wheel control torque input, s the Laplace transform variable, I the spacecraft inertia, K_i the ith flexible mode gain, ω_i the ith flexible mode frequency in rad/sec, ζ is the passive damping ratio assumed as 0.005. Table 2 lists the pitch/yaw axes modal data of the HST.

The baseline PID controller for each axis, not including a roll-off filter in the rate loop [15-17], is given by

$$u(s) = -I(K_P + K_I/s + K_D s)\theta(s)$$

where $K_P = 9$, $K_I = 0.45$, and $K_D = 4.5$ for both pitch and yaw axes. The controller is digitally implemented with a 25 msec sampling period and the control loop has a 7 msec pure time delay.

The following new controller with two dipoles is proposed for the HST to accommodate both the 0.12 Hz and 0.66 Hz disturbances:

$$\frac{u(s)}{\theta(s)} = -I(K_P + K_I/s + K_D s) \times 0.5 \frac{[(s/z_1)^2 + 2\zeta_{z_1} s/z_1 + 1][(s/z_2)^2 + 2\zeta_{z_2} s/z_2 + 1]}{[(s/p_1)^2 + 2\zeta_{p_1} s/p_1 + 1][(s/p_2)^2 + 2\zeta_{p_2} s/p_2 + 1]}$$

where

$$z_1 = 2\pi(0.08),\ \zeta_{z_1} = 1.00$$
$$p_1 = 2\pi(0.12),\ \zeta_{p_1} = 0.01$$
$$z_2 = 2\pi(0.50),\ \zeta_{z_2} = 0.20$$
$$p_2 = 2\pi(0.66),\ \zeta_{p_2} = 0.01$$

and the overall loop gain is not reduced by a factor of two if only one dipole is employed.

Figure 8 shows a direct comparison of the closed-loop frequency responses from the yaw-axis disturbance to the pitch attitude output for three different cases: 1) the baseline PID controller, 2) PID + one dipole at 0.12 Hz, and 3) PID + two dipoles. It can be seen that as compared to the baseline PID controller, the new controller with one dipole has a 40 dB more gain attenuation at 0.12 Hz and an additional 10 dB attenuation at 0.66 Hz without significantly affecting the low- and high-frequency gains. The new proposed controller with two dipoles has additional 40 dB gain attenuation at both 0.12 Hz and 0.66 Hz, as compared to the baseline PID controller. As can be seen in Fig. 9, the proposed controller with two dipoles has the same 1.5-Hz bandwidth as the baseline PID controller. The high-frequency structural modes near 14 Hz are in fact phase-stabilized by the phase lag effects of the sampling and time delay.

7. Conclusions

The experimental results for the ACES structure located at the NASA Marshall Space Flight Center have been presented. The primary objective of verifying the simplicity and effectiveness of the classical single-loop-at-a-time approach for controlling a

complex flexible structure such as the ACES has been accomplished. The simplicity and practicality of the "dipole" concept for persistent disturbance rejection control of flexible structures was successfully demonstrated.

Acknowledgments

This research was supported by the NASA Langley Research Center under the Control Structure Interaction (CSI) Guest Investigator Program. The author would like to thank Dr. Henry Waites and Mr. John Sharkey at the NASA Marshall Space Flight Center for their efforts in developing such an excellent test facility and for their technical assistance during tests. The technical support of Mr. Michael Dendy of Control Dynamics Company during tests is also acknowledged. The author is also very grateful to Mr. Jerry Newsome (CSI Program Manager) and Ms. Rudeen Smith-Taylor (CSI GI Program Manager) for supporting the advancement of classical control theory as applied to the CSI technology.

Appendix: Classical SISO Design Approach

In this appendix, a classical SISO control design approach, with special emphasis on a generalized structural filtering concept [12] and a dipole concept [13], is summarized.

Successive-Mode-Stabilization

The design of a SISO feedback control system for a flexible structure is carried out starting with the stabilization of a rigid-body mode and/or dominant flexible modes and subsequent analysis and stabilization of unstably interacting flexible modes. Feedback control with a non-colocated actuator and sensor pair or with significant time delay generally results in the presence of unstably interacting flexible modes. After the unstably interacting modes have been identified, proper filtering to phase or gain stabilize those modes is then introduced. Also, active disturbance rejection filtering is synthesized to compensate for any persistent disturbances acting on the structure. Aided by the root locus method and/or Bode plots, and a certain amount of trial and error, a robust compensator design is obtained.

The classical SISO design based on successive-mode-stabilization can be divided into four steps:

1) Stabilization of a rigid-body mode and/or dominant flexible modes according to given time- or frequency-domain specifications (settling time, maximum overshoot, bandwidth, phase and gain margins).

2) Gain/phase stabilization of any unstably interacting or destabilized flexible modes.

3) Synthesis of active disturbance rejection filter and/or command preshaping filter.

4) Final tuning of the overall compensator.

The last step becomes necessary because the phase and gain characteristics of active disturbance rejection filtering as well as the stabilized modes in question exert their influence on all neighboring frequencies, which may include other modes. This presents a challenge as the number of modes to be stabilized becomes larger.

Phase and/or gain stabilization of an unstably interacting flexible mode can be achieved with the introduction of a roll-off filter and/or a generalized second-order filter of the following form in the feedback loop:

$$\frac{(s/z)^2 + 2\zeta_z s/z + 1}{(s/p)^2 + 2\zeta_p s/p + 1}$$

where s is the Laplace transform variable. Non-minimum-phase second-order shaping filters with negative ζ_z are of special interest for a certain class of noncolocated control problems, as discovered in [12].

Active Disturbance Rejection

After successful stabilization of the rigid-body mode and/or dominant flexible modes (as well as any other unstably interacting flexible modes), active disturbance rejection is then simply achieved by introducing into the feedback loop a disturbance model of the form

$$w(t) = \sum_i A_i \sin(p_i t + \phi_i)$$

with unknown magnitudes A_i and phases ϕ_i but known frequencies p_i. In general, the disturbance $w(t)$ can be described by a Laplace transformation $w(s) = N_w(s)/D_w(s)$, where $N_w(s)$ is arbitrary as long as $w(s)$ remains proper. The roots of $D_w(s)$ correspond to the frequencies at which the persistent excitation takes place. The inclusion of the disturbance model $1/D_w$ inside the control loop is often referred to as the internal modeling of the disturbance.

The presence of $1/D_w$ in the control loop results in the effective cancellation of the poles of $w(s)$, provided that no root of $D_w(s)$ is a zero of the plant transfer function.

This is shown in the following closed-loop transfer function :

$$y(s) = \frac{1/D(s)}{1 + N_c(s)N(s)/D_c(s)D_w(s)D(s)} w(s)$$
$$= \frac{D_c(s)D_w(s)}{D_w(s)D_c(s)D(s) + N_c(s)N(s)} \frac{N_w(s)}{D_w(s)}$$

where we can see the cancellation of $D_w(s)$.

The compensator can be viewed as a series of individual first-order or second-order filters as follows:

$$\frac{N_c(s)}{D_c(s)} = \prod_i \frac{N_{c_i}(s)}{D_{c_i}(s)}$$

Each filter is designed to perform a specific task, like the stabilization of a particular mode. In the same manner, a disturbance rejection filter can be designed that has a proper transfer function and uses the internal disturbance model $1/D_w$. Thus a proper numerator is chosen in the compensator to go with the disturbance model. The numerator is chosen to be of the same order as D_w so that there is a zero for each pole of the disturbance model $1/D_w$.

Each pole-zero combination of the disturbance rejection filter

$$\prod_i \frac{(s/z_i)^2 + 2\zeta_{z_i} s/z_i + 1}{(s/p_i)^2 + 1}$$

can be called a *dipole*, where ζ_{z_i} is included for generality. The filter thus consists of as many dipoles as there are frequency components in the persistent disturbance. The separation between the zero and the pole is generally referred to as the strength of the dipole. The strength of the dipole affects the settling time of the closed-loop system; in general, the larger the separation between the pole and zero of the filter the shorter the settling time. This is caused by the position of the closed-loop eigenvalue corresponding to the filter dipole. As the strength of the dipole is increased, this eigenvalue is pushed farther to the left, speeding up the response time of the disturbance rejection. Therefore, as the strength of the dipole is changed to meet a chosen settling time the compensation must be readjusted. A compromise has to be reached often between the the settling time and the stability of the compensated system.

References

[1] Newsome, J.R., et al., "The NASA Controls-Structures Interaction Technology Program," IAF-90-290, *41st Congress of the International Astronautical Federation,* October 6-12, GDR, 1990.

[2] Waites, H., et al., "Active Control Technique Evaluation for Spacecraft (ACES)," Final Technical Report, F33615-86-C-3225, NASA/MSFC and Control Dynamics Company, March 25, 1988.

[3] Pearson, J. and Waites, H., "Advanced Control Evaluation for Structures (ACES) Programs," *Proceedings of the 1988 American Control Conference*, June 15-17, 1988, pp. 1448-1452.

[4] Jones, V.L. and Waites, H., "ACES Program: Lesson Learned," *Proceedings of the 1988 American Control Conference*, June 15-17, 1988, pp. 1453-1455.

[5] Irwin, R.D., "Application of FAMESS to a Large Space Structure Ground Test Facility," *Proceedings of the 1988 American Control Conference*, June 15-17, 1988, pp. 1456-1461.

[6] Collins, E.G., Phillips, D., and Hyland, D.C., "Design and Implementation of Robust Decentralized Control Laws for the ACES Structure," *Proceedings of the 1990 American Control Conference*, May 23-25, 1990, pp. 1449-1454.

[7] Slater, G., et al., "Practical Experience with Multivariable Positivity Controllers for the ACES," *Proceedings of the 1990 American Control Conference*, May 23-25, 1990, pp. 1445-1448.

[8] Balas, G. and Doyle, J., "Caltech CSI GI Year End Review," NASA CSI Guest Investigator First Year Review Meeting, Jan. 23-24, 1990, NASA Langley Research Center, pp. 479-550.

[9] Liu, K. and Skelton, R., "Experimental Verification of an Integrated Modeling and Control Strategy for Flexible Structures," NASA CSI Guest Investigator Final Review Meeting, April 5, 1991, Huntsville, AL, pp. 121-178.

[10] Wie, B., "Experimental Verification of a Classical SISO Approach to Flexible Structure Control," NASA CSI Guest Investigator Final Review Meeting, April 5, 1991, Huntsville, AL, pp. 179-218.

[11] Wie, B., "Active Vibration Control Synthesis for the COFS Mast Flight System," *Journal of Guidance, Control, and Dynamics*, Vol.11, No.3, 1988, pp. 271-276.

[12] Wie, B. and Byun, K., "New Generalized Structural Filtering Concept for Active Vibration Control Synthesis," *Journal of Guidance, Control, and Dynamics*, Vol.12, No.2, 1989, pp. 147-154.

[13] Wie, B. and Gonzalez, M., "Control Synthesis for Flexible Space Structures Excited by Persistent Disturbances," AIAA Paper No. 90-3427, to appear in the *Journal of Guidance, Control, and Dynamics.*

[14] Wie, B., Horta, L., and Sulla, J., "Classical Control System Design and Experiment for the Mini-Mast Truss Structure," *Proceedings of the 1990 American Control Conference*, May 23-25, 1990, pp. 1428-1434, also *Journal of Guidance, Control, and Dynamics*, Vol. 14, No. 4, 1991, pp. 778-784.

[15] "Hubble Space Telescope SAGA Readiness Review Report," NASA Goddard Space Flight Center, October 2, 1990.

[16] Dougherty, H., et al., "Space Telescope Pointing Control System," *Journal of Guidance, Control, and Dynamics*, Vol.5, No.4, 1982, pp. 403-409.

[17] Beals, G.A., et al., "Hubble Space Telescope Precision Pointing Control System," *Journal of Guidance, Control, and Dynamics*, Vol.11, No.2, 1988, pp. 119-123.

[18] Wie, B., Liu, Q. and Bauer, F., "Classical and Modern Control Redesign for the Hubble Space Telescope," to be presented at the 1992 AIAA Guidance, Navigation, and Control Conference.

Table 1: ACES Structural Mode Description

Mode (Hz)	Description
0.14	1st Astromast X-Bending
0.15	1st Astromast Y-Bending
0.63	2nd Astromast Y-Bending
0.75	2nd Astromast X-Bending
0.82	3rd Astromast Y-Bending
1.04	3rd Astromast X-Bending
1.41	Antenna Torsion
1.51	IMC Gimbals
2.35	Antenna Torsion + Astromast Bending
2.49	Antenna Torsion + Astromast Bending
2.73	Astromast Bending

Table 2: HST Modal Data (Pitch/Yaw Axes)

Mode Number	ω_i (Hz)	Modal Gain (K_i) Pitch	Yaw
1	0.120	0.018	0.025
2	0.432	0.012	0.000
3	0.660	0.000	0.079
4	0.912	0.057	0.000
5	1.079	0.000	0.029
6	2.508	0.000	0.013
7	10.834	0.024	0.104
8	12.133	0.155	-0.320
9	13.201	-1.341	-0.110
10	14.068	-1.387	-0.217
11	14.285	-0.806	-1.516
12	15.264	-0.134	0.170

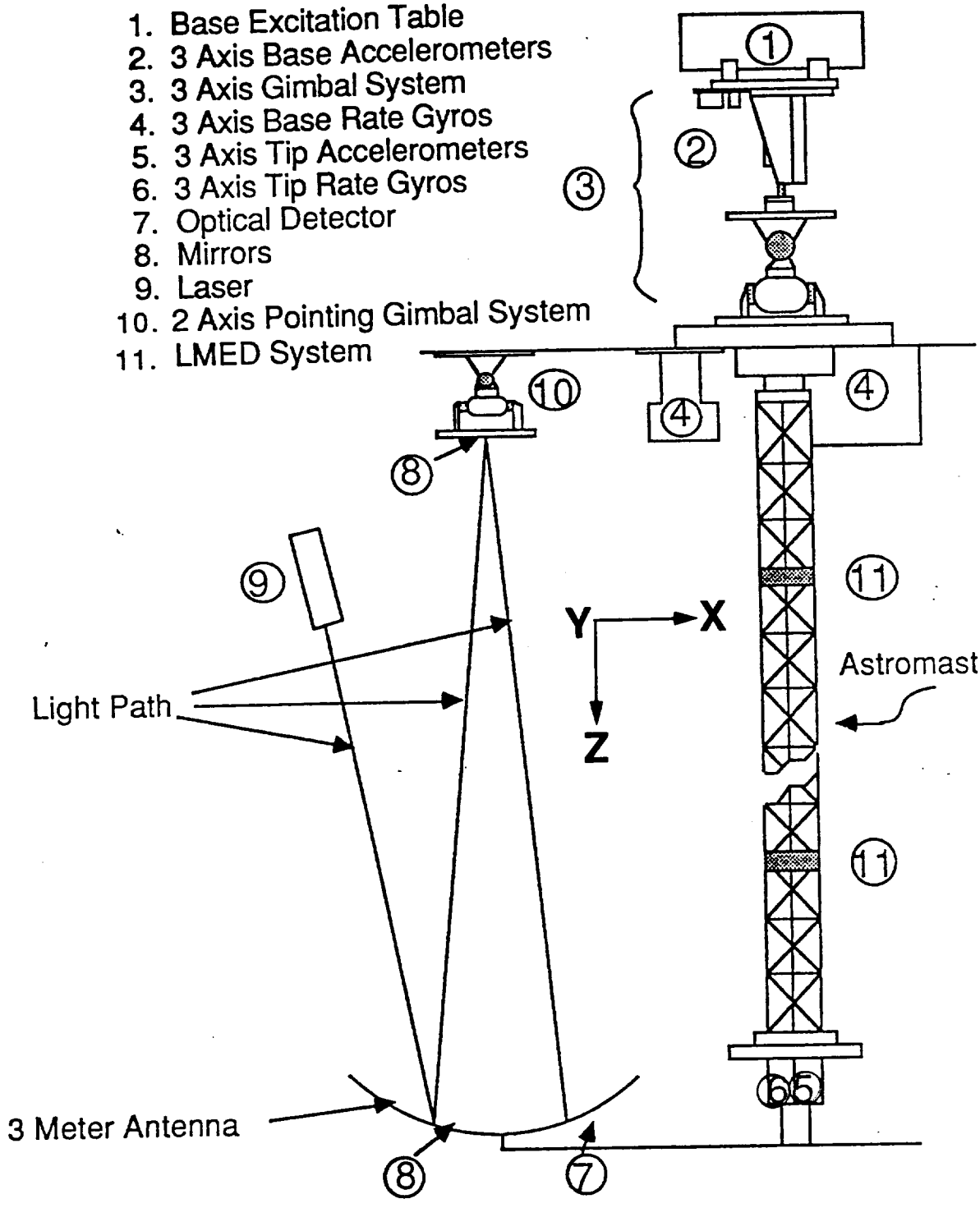

Figure 1. The ACES Ground Test Facility

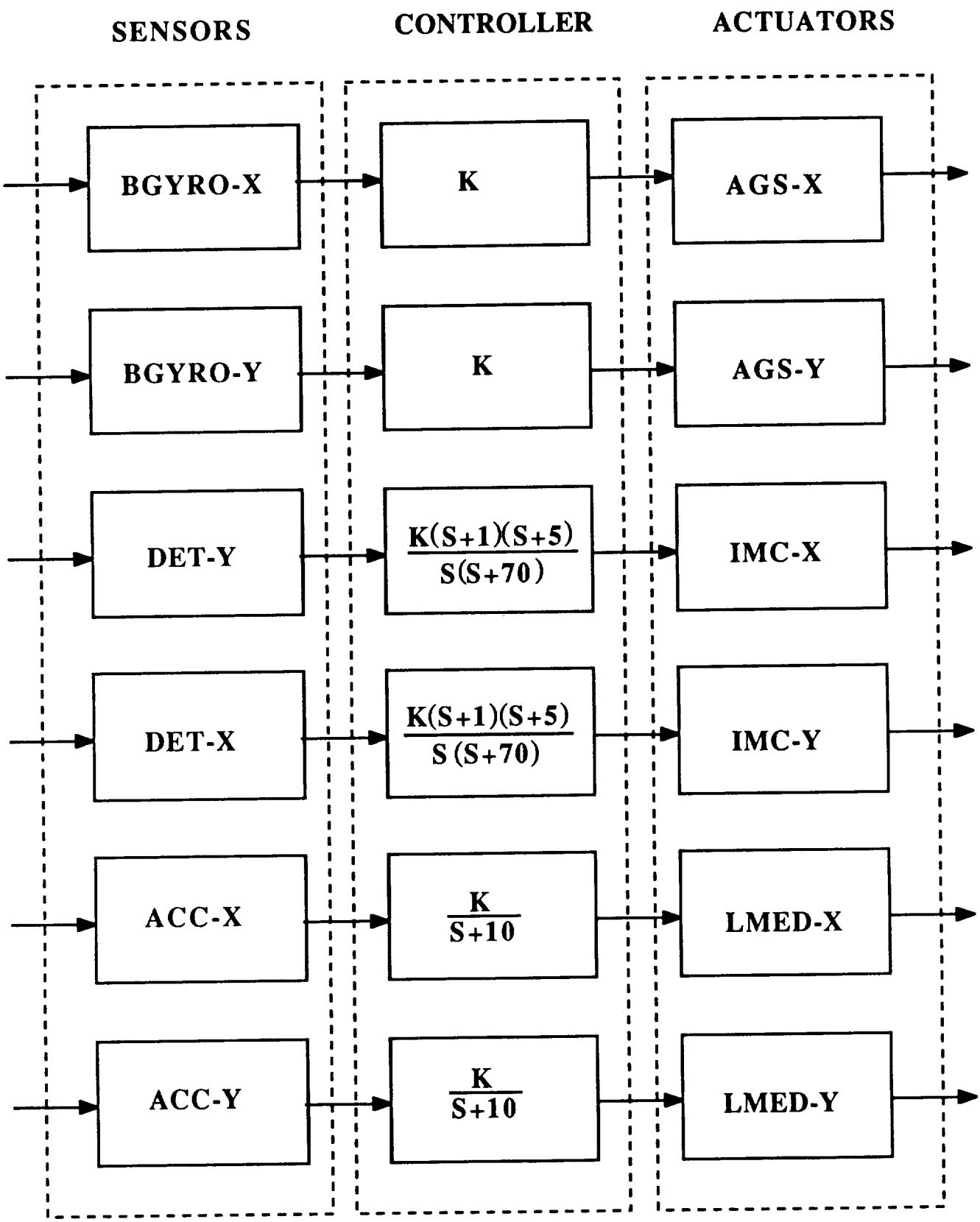

Figure 2. Classical SISO Controller for the ACES

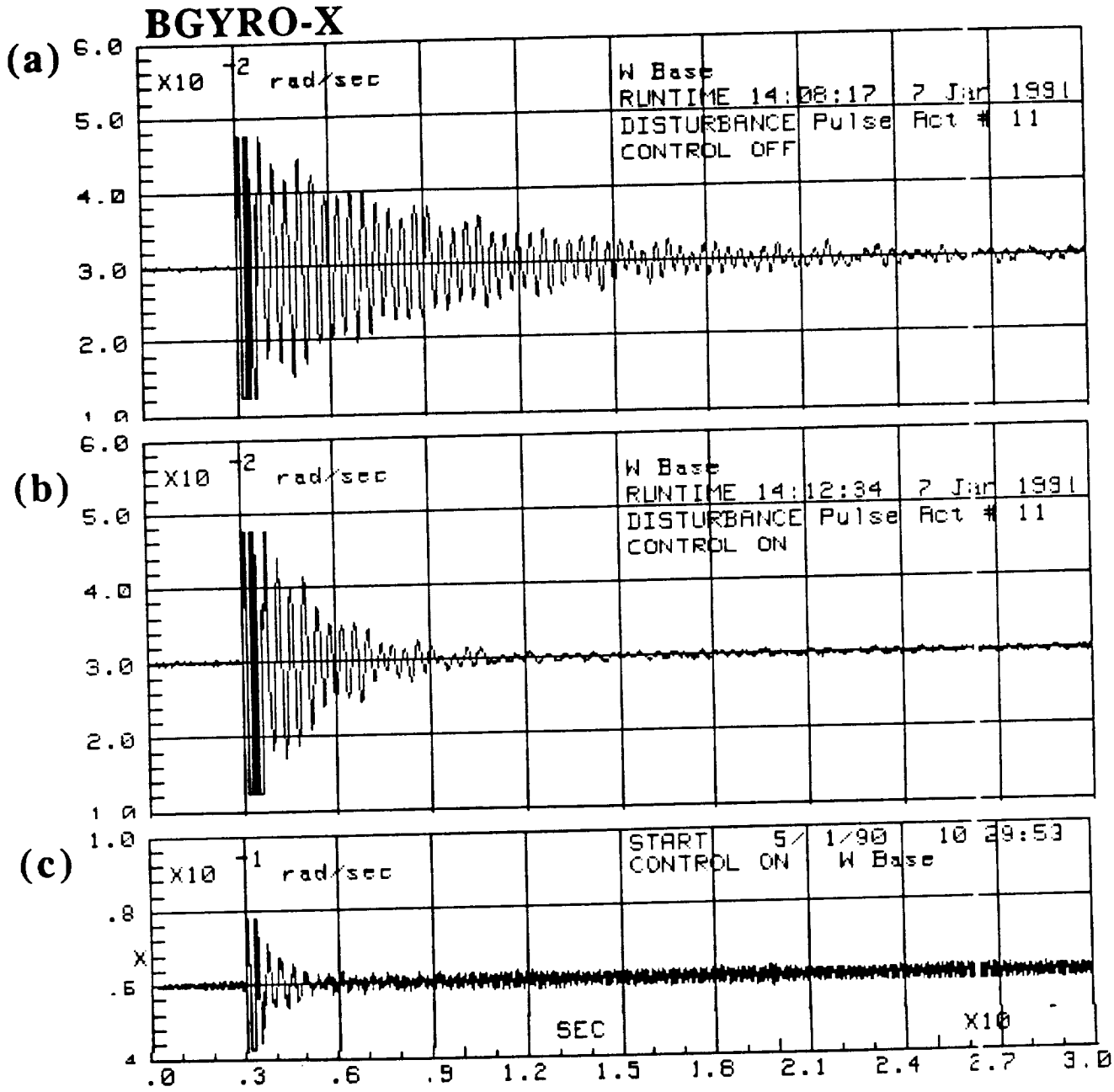

Fig. 3. BGYRO-X Responses to BET-Y Pulse: (a) Open-Loop, (b) AGS Closed-Loop with Nominal Gain, (c) AGS Closed-Loop with High Gain

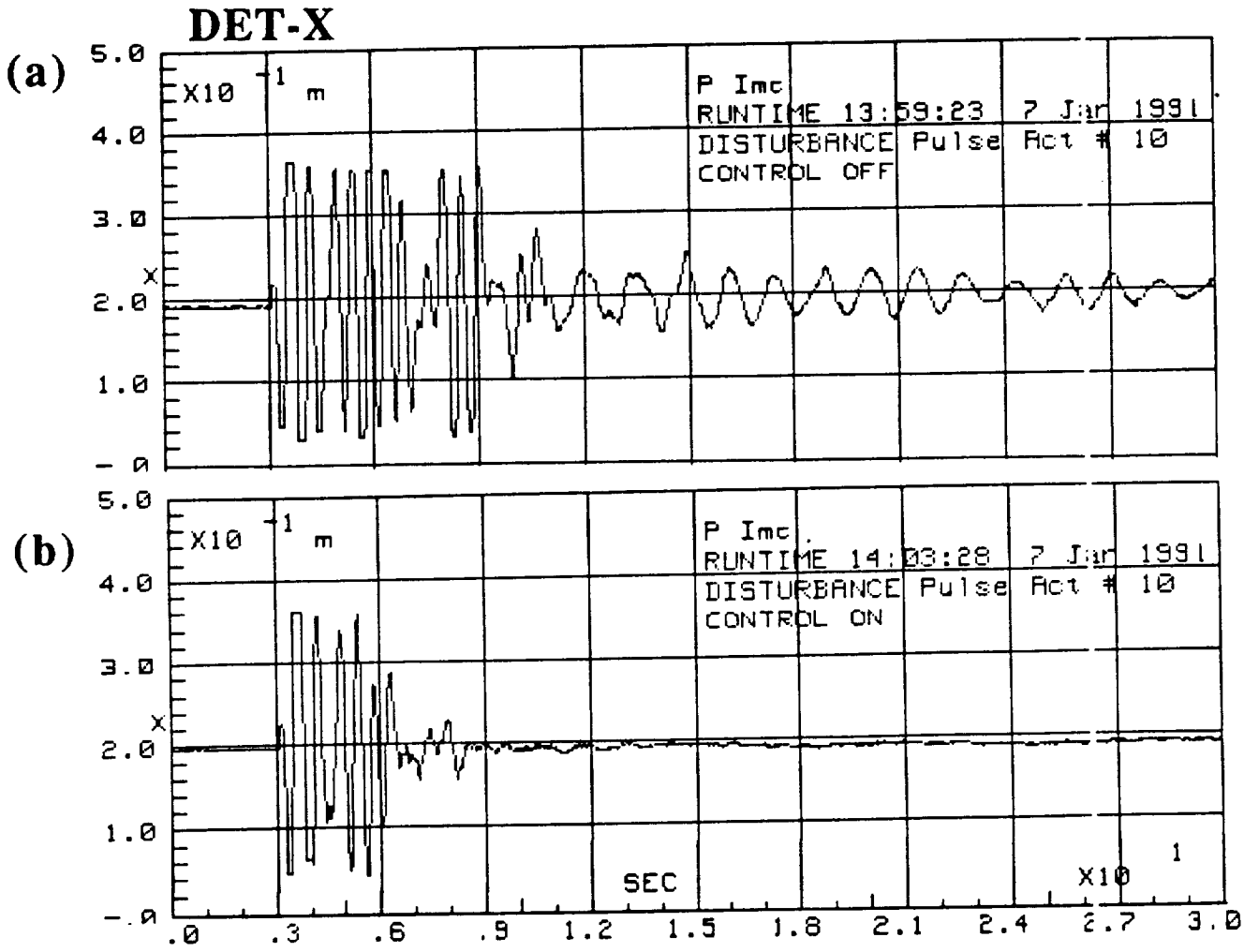

Fig. 4. DET-X Responses to BET-X Pulse: (a) Open-Loop and (b) AGS Closed-Loop with Nominal Gain

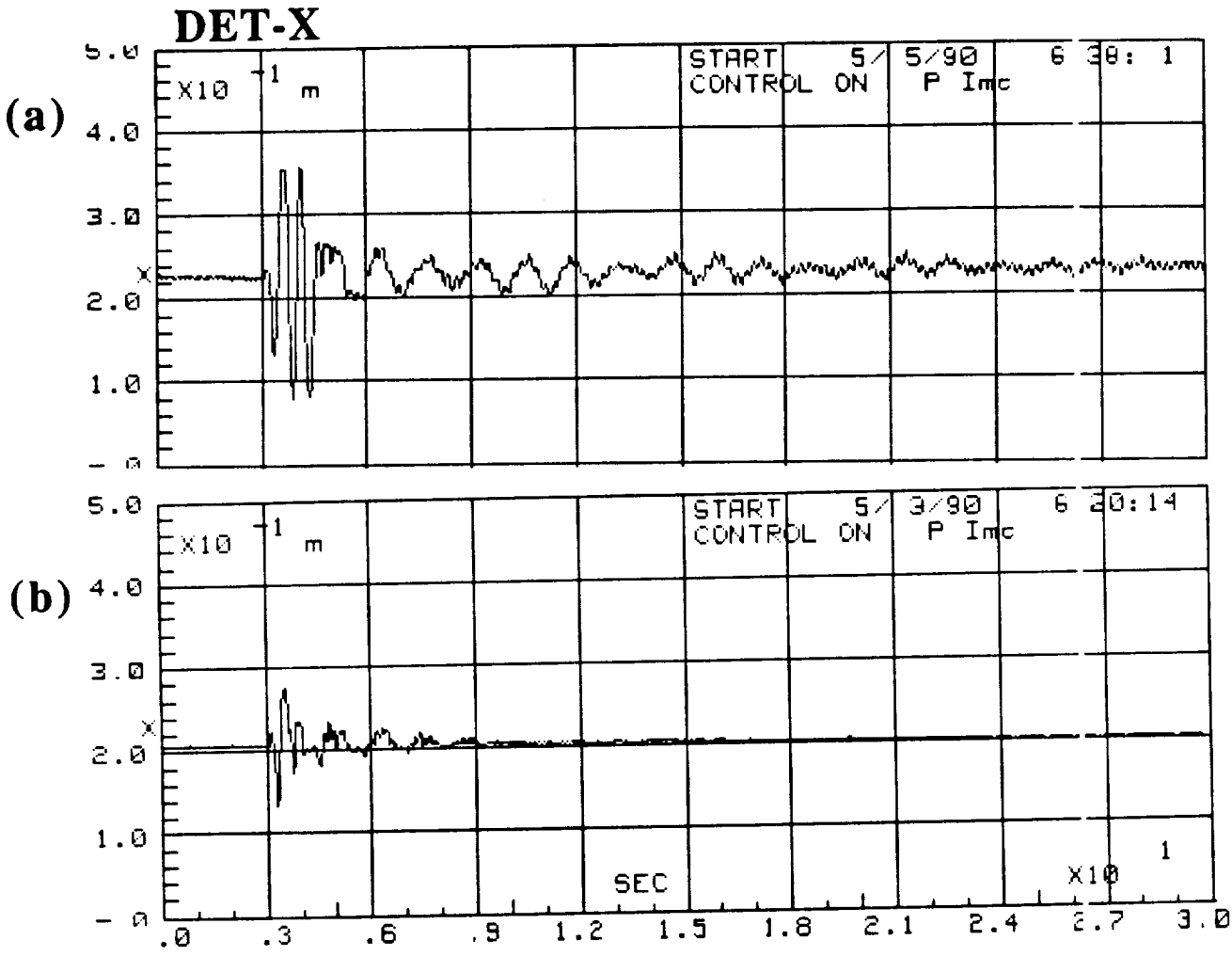

Fig. 5. DET-X Responses to BET-X Pulse: (a) LMED Closed-Loop and (b) AGS + IMC Closed-Loop with Nominal Gain

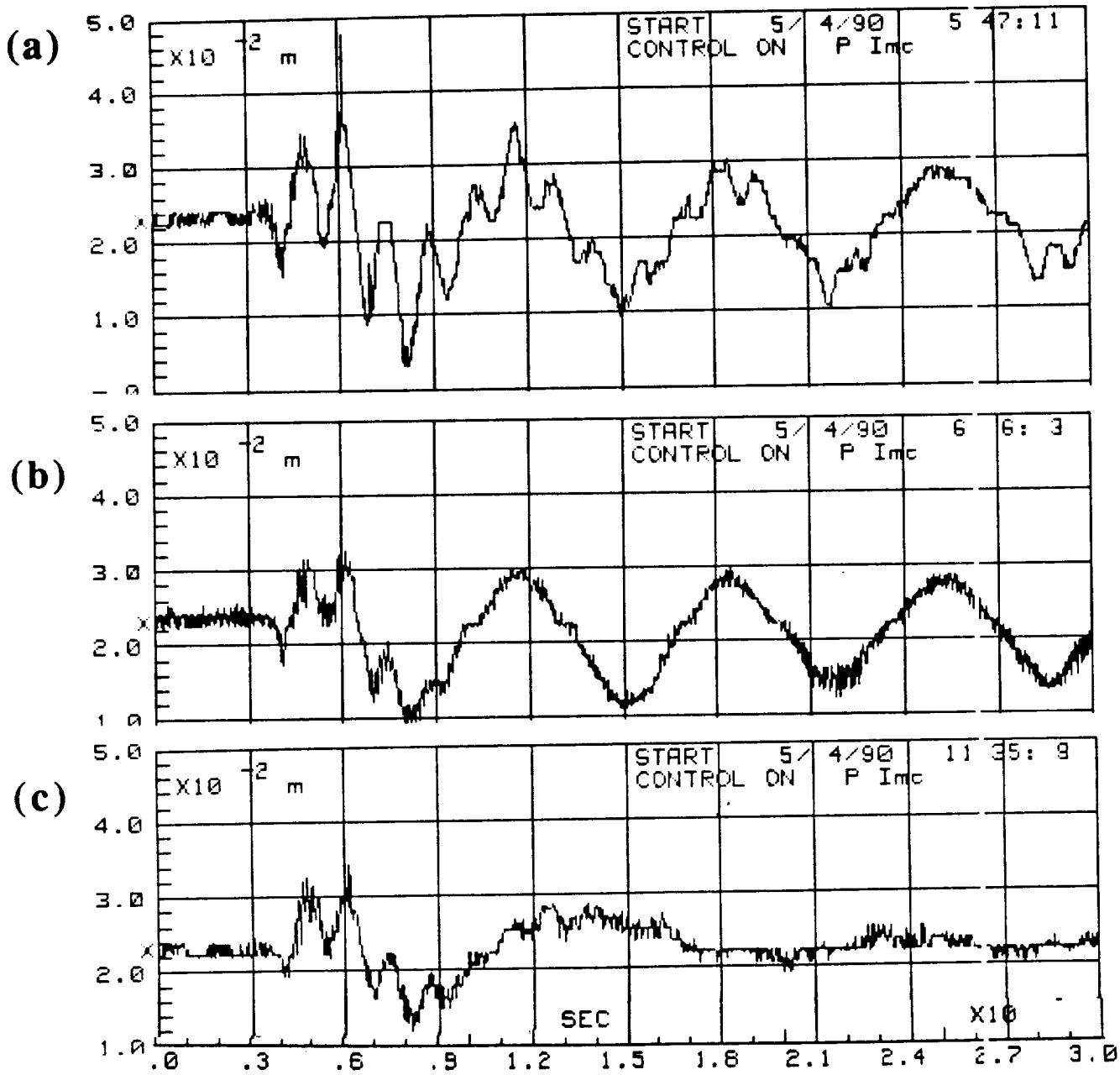

Fig. 6. DET-X Responses to BET-X Step: (a) Open-Loop, (b) AGS + IMC (Fig. 2) and (c) AGS + IMC (Fig. 7 with Periodic-Disturbance Rejection Dipole)

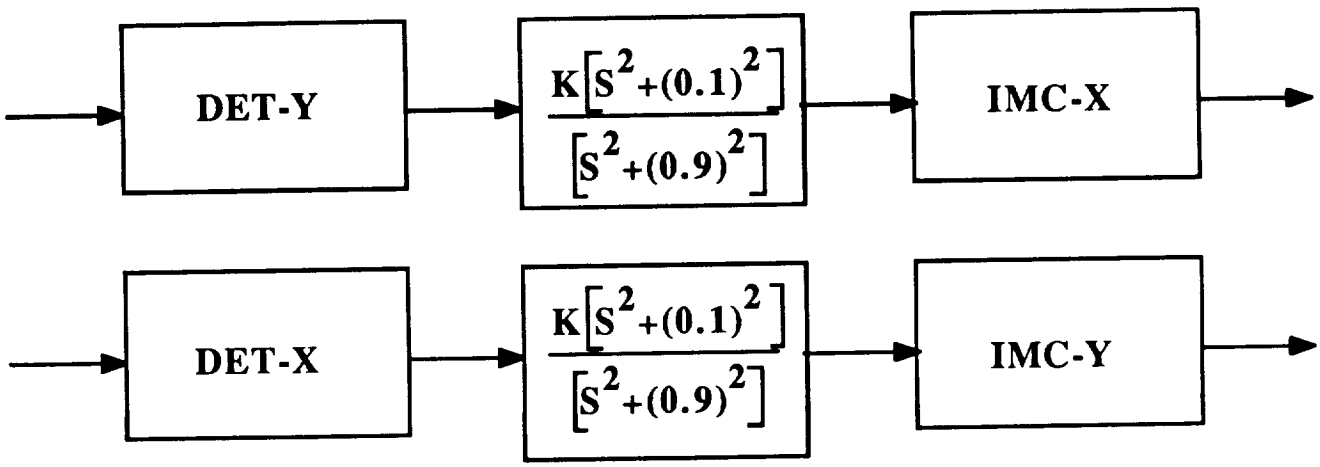

Fig. 7. IMC Controller with Periodic-Disturbance Rejection Dipole

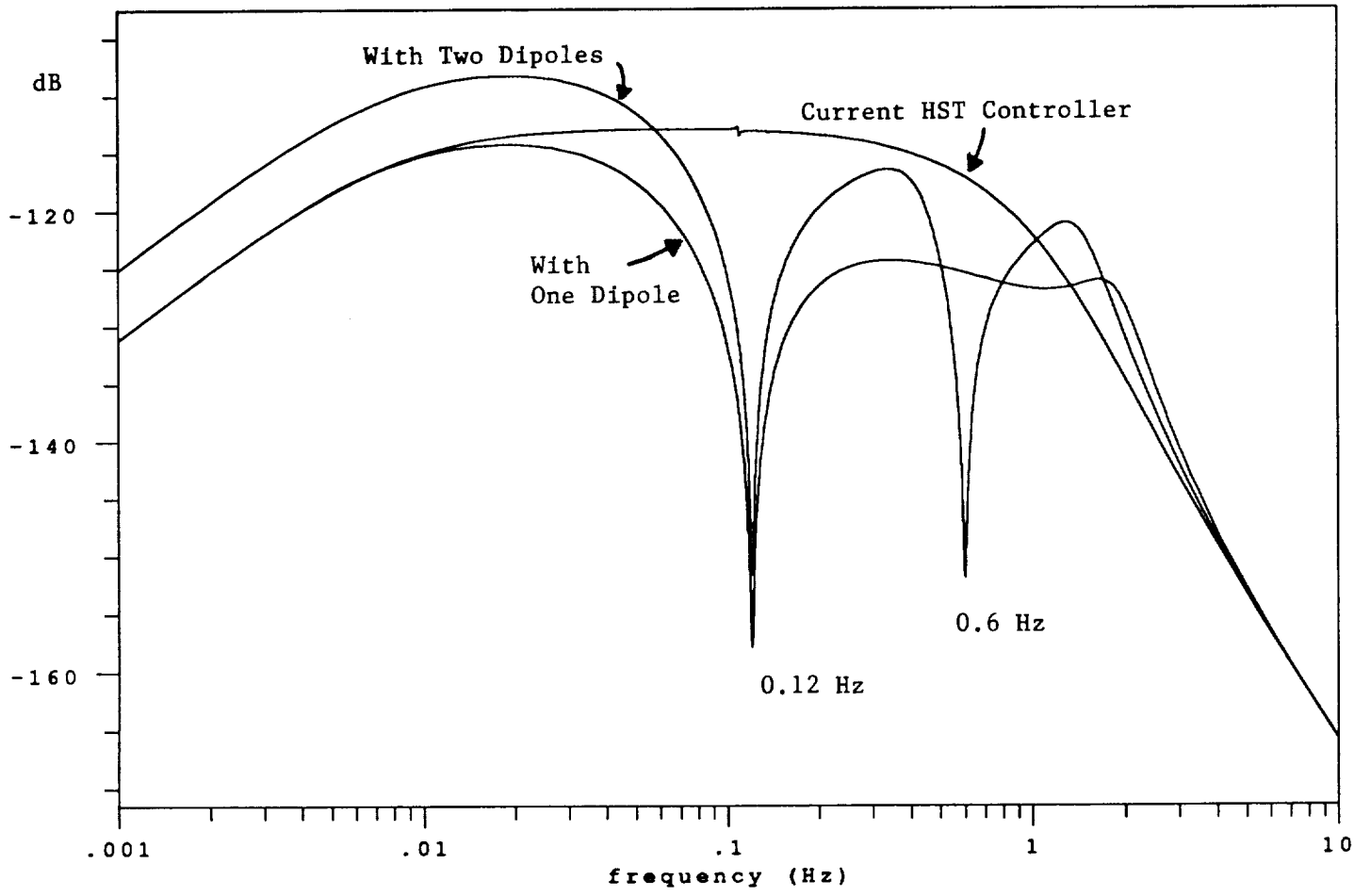

Fig. 8. Closed-Loop Bode Magnitude Plots for the Hubble Space Telescope

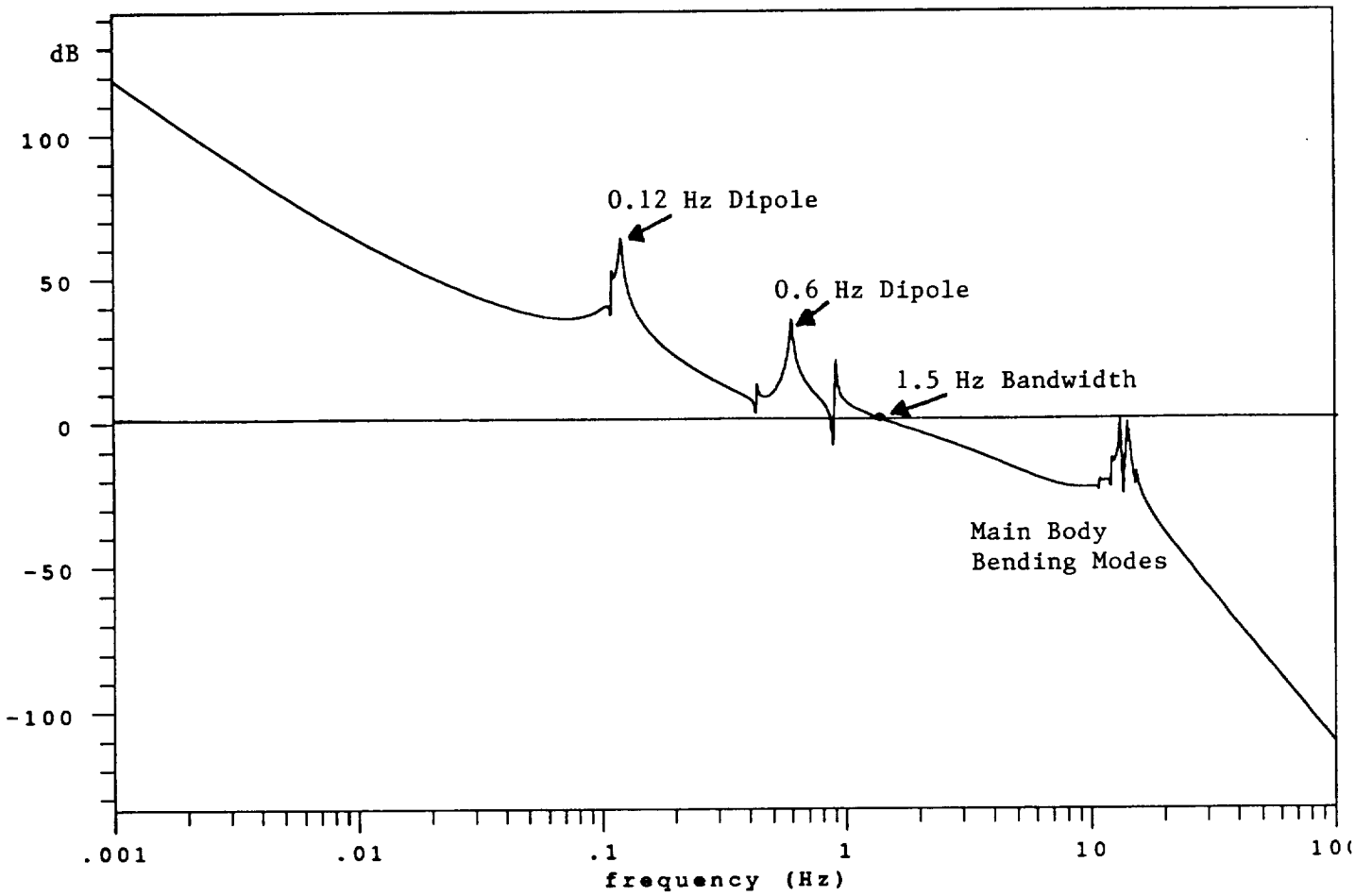

Fig. 9. Loop Transfer Function Magnitude Plot for a Proposed Controller with Two Dipoles for Disturbance Rejection at 0.12 Hz and 0.66 Hz.